An Experimental Study of Traction Characteristics for a Family of Transmission Fluids

Undergraduate Honors Thesis

Presented in Partial Fulfillment of the Requirements for Graduation with Honors Research Distinction in the Department of Mechanical Engineering at The Ohio State University

By

Colton Thomas

Undergraduate Honors Program in Mechanical Engineering

The Ohio State University

2020

Thesis Committee

Dr. Ahmet Kahraman, Advisor

Dr. Michael Handschuh, Co-Advisor

Dr. David Talbot

ABSTRACT

Efficiency of transmissions used in ground vehicles is a major research topic in automotive industry, aiming at increasing the travel distance and life of hybrid or electric vehicles. Any achievable reductions in power losses of the transmission results directly in improved fuel economy or battery driving range for a typical internal combustion engine or electric vehicle, respectively. As such, establishing friction characteristics of transmissions fluid empirically becomes critical for conducting direct comparisons between different fluids. These friction measurements can be regressed into friction formulae to be used in simplified power loss prediction models, while also providing much needed data for validation of more advanced tribology models. In this study, a methodology is proposed to perform tightly controlled traction measurements of lubricated contacts of a two-disk tribometer setup. This methodology is applied to three candidate transmission fluids identified for a high-speed automotive application to provide a comparison amongst them. Traction curves are generated for each lubricant covering wide ranges of contact parameters including rolling and sliding velocities, normal force, and oil inlet temperature. Finally, these curves are regressed to derive closed-form friction formulae for each lubricant as a function of the same parameters.

DEDICATION

This is dedicated to my family and friends.

ACKNOWLEDGEMENTS

I would like to express special thanks of gratitude to Dr. Ahmet Kahraman for providing me the opportunity to work in the Gear and Power Transmission Research Laboratory. I also wish to thank him for allowing me to further my education and work as a graduate research assistant while I complete my master's degree.

I am also very much thankful and express sincere appreciation for Dr. Michael Handschuh for letting me work alongside him the past two and a half years, providing guidance, being patient, and pushing me to be a better student, friend, and colleague each and every single day.

I sincerely thank the other undergraduate and graduate students, and specifically Emily Aneshansley, Robert McEwan, and Zach Teaford, for their endless help along the way.

Lastly, I would like to thank my parents, grandparents, and friends for encouraging and motivating me to stay focused and complete this project. I am fortunate to be surrounded by amazing family and friends, and extremely grateful for my friend Nikki Mehalic for her assistance with various academic projects throughout the duration of this study.

VITA

December 12, 1997 ..... Born – Canton, Ohio

May 2016 ..... New Philadelphia High School
New Philadelphia, Ohio

May – August 2017 ..... Mechanical Engineering Intern
Allied Machine and Engineering
Dover, OH

June – August 2018 ..... Mechanical Engineering Intern
Oshkosh Corporation
Oshkosh, WI

May – August 2019 ..... Externals Design Engineering Intern
Pratt and Whitney
East Hartford, CT

September 2018 – December 2020 ..... Undergraduate Research Associate
GearLab
The Ohio State University
Columbus, OH

Fields of Study

Major Field: Mechanical Engineering

TABLE OF CONTENTS

LIST OF TABLES

LIST OF FIGURES

NOMENCLATURE

Symbol	*Definition*	*Unit*
E_i	Modulus of elasticity	GPa
c_i	Specific heat	J/kg/K
h	Lubricant film thickness	µm
r_i	Disk radius	mm
Ra	Arithmetic surface roughness average	µm
Rq	Root mean square of surface roughness	µm
F	Contact normal force	N
F_f	Friction force	N
SR	Slide-to-roll ratio	--
T_i	Measured contact torque	Nm
T_c	True contact torque	Nm
$T_{f,i}$	Friction torque	Nm
$T_{b,i}$	Roller element torque losses	Nm
$T_{s,i}$	spin torque losses	Nm
u_i	Disk surface velocity	m/s
u_r	Rolling (entrainment) velocity	m/s
u_s	Sliding (entrainment) velocity	m/s
β_i	Regression coefficient	--
ε	Error term	--
η	Lubricant viscosity	Pas
ν_i	Poisson's ratio	--

$\theta_{b.i}$	Surface bulk temperature	°C
θ_{lube}	Inlet lubricant temperature	°C
κ_i	Thermal conductivity	W/m/K
μ	Coefficient of friction	--
$\bar{\mu}$	Average coefficient of friction	--
ρ_i	Density	kg / m^3
σ_{Herztian}	Maximum Hertzian contact pressure	GPa
τ	Shear stress	GPa
Ω_i	Disk speed	rpm

Subscripts

i	Disk surface

CHAPTER 1

INTRODUCTION

1.1 Background and Motivation

Depleting fossil fuels combined with environmental concerns are forcing the automotive industry to consider electric vehicles as the future mode of transportation in place of vehicles powered by internal combustion engines. In terms of transmission engineering, this shift represents significant technical challenges as the transmissions of electric vehicles much handle input speeds four to ten times higher than those experienced by today's conventional manual or automatic transmissions. At such high speeds, gears must be lubricated by lower viscosity fluids that cause limited churning power losses, at the same time, having superior low-friction characteristics for reducing load-dependent power losses and heat generation at the gear meshes.

Tribometers are popular devices used to simulate the operating conditions seen in typical gearing applications under controlled conditions, making them useful for gearbox power loss investigations. Generally, well-designed tribometers are equipped with

measurement devices that allow for precise measurement of friction and can monitor and control other relative factors relating to friction measurements, such as temperature, load, and velocity, covering a specific ranges of testing parameter suitable for various applications.

New generation transmission fluids are being marketed by oil industry with the claim that they are optimal for higher speed automotive transmissions. No direct experimental comparison of these transmission fluids for their friction characteristics is readily available. Likewise, elastohydrodynamic lubrication (EHL) models equipped with stated rheological properties of these fluids lack validation since no objective friction coefficient data is available for comparison.

1.2 Literature Review

Performing experiments to measure friction coefficients of contacts lubricated with various fluids have been done in the past using various types of tribometers. These machines include, but are not limited to, ball-on-disk [1–4] , ball-on-prism [5], and two-disk setups [6–10]. The idea is to subject the lubricated contact to a given rolling and sliding velocity, normal force, and lubricant inlet temperature while measuring the traction torque and surface bulk temperature generated by the friction at this rolling-sliding condition. Ball-on-disk machines operate by spinning a ball against a flat, horizontal disk as a load is applied to the ball via a cantilever beam and can achieve non-collinear surface velocities, mimicking hypoid surface velocities for instance. Two-disk machines have parallel axes and rotate against each other to achieve colinear rolling and sliding velocities which are seen in spur and helical gear contacts.

Most of these test machines are capable of operating at automotive conditions for which the powertrain is a standard internal combustion engine (i.e. moderate speeds and temperatures) [5,6,8,11,12]. Liou [6] and Wilson [8] operated a twin-disk setup that could achieve a maximum rolling velocity of 15 m/s with their respective disks. Others tested non-automotive fluids under conditions more representative of aerospace contact conditions (i.e. high speeds and temperatures) [7,9,10]. Patching et al. [9] tested aerospace lubricants with rolling velocities up to 21 m/s and inlet temperatures of 100°C. Handschuh et al. [7] developed a tribometer capable of reaching rolling velocities of 56 m/s and oil inlet temperatures of 160°C, testing automotive lubricants up to 15 m/s at 90°C and aerospace lubricants up to 50 m/s at 121°C. Such high-speed machines provide the capability for experimental evaluation of new-generation automotive transmission fluids under high speeds suitable for electric vehicle operation.

Aside from the previously mentioned operating conditions (i.e. speed and temperature), automotive gearing applications usually have rougher surfaces. These contact conditions (i.e. low speed, high-load, and rough surfaces) lead to increased asperity contact which directly influences the overall friction coefficient of the contact. There has been numerous gear [13–15] and twin-disk tribometer [6,16,17] experiments showing that a reduction in surface roughness reduce mechanical power losses. Petry-Johnson et al. [15] found that mechanical power losses were reduced by 19% between ground and chemically polished gears. Diab et al. [16] used a twin disk machine comparing traction behavior at low operating speeds between ground and polished disk surfaces. Thus, to accurately isolate the friction performance of a lubricant, the surface roughness must be reduced and controlled.

Experimental traction tests lend themselves for statistical analysis. Many regression analyses of traction measurements covering a wide range of operating conditions exist within the literature [18–22] from tribometers. These friction coefficient empirical formulae for rolling-sliding contacts are influenced by several parameters: load (pressure), rolling velocity, sliding velocity, surface roughness, radii of curvature, and lubricant viscosity and often have an applicable range. For instance, Drozdov and Gavrikov [19] developed and empirical formula quantifying kinematic viscosity up to 4.5 Pas, rolling and sliding velocity range between 5 and 20 m/s, and contact pressures up to 1.9 GPa. Benedict and Kelley [18] quantified surface roughness, load, dynamic viscosity, and sliding and rolling velocity within their empirical formulae, which has a surface roughness range up to 0.8 micrometers.

Various transmission fluids will be evaluated in this study using a high-speed two-disk tribometer developed by Handschuh et al. [7]. Regression of the measured traction curves for each lubricant in a form similar to Xu et al. [21] will allow for closed-form formulae for the friction coefficient, which is expected to be convenient for comparison of transmission fluids at any given operating condition as well as providing the experimental database for thermal-EHL models such as the one developed by Li et al. [2] for assessing their capability of modeling these new-age fluids.

1.3 Scope and Objectives

From the literature review, the field of study is currently lacking experimental data of the friction characteristics of new-age automotive transmission fluids operating at

aerospace contact conditions suitable for electric vehicle operation. As such, the specific objectives of this study are as follows:

- Establish a suitable experimental methodology for quantifying friction along rolling-sliding lubricated contacts.
- Perform traction measurements for a family of automotive transmissions fluids within realistic ranges of operating parameters, namely rolling and sliding velocity, lubricant inlet temperature and contact pressure.
- Apply regression techniques to the measured data to derive closed-form friction formula for each transmission fluid.

Super-finished (chemically polished) disk specimens will be used to limit the influence of surface roughness on traction torque to better characterize and isolate the friction characteristics of each transmission fluid.

1.4 Thesis Outline

The contents of this thesis are outlined below. Chapter 2 describes the high-speed, twin-disk tribometer along with its critical components and measurement systems. Disk specimen properties are defined. The contact torque isolation procedure is summarized. Details of the traction test protocol and test matrix are outlined along with the inspection procedure. The experimental traction tests are presented in Chapter 3. Results from selected test conditions compare the friction characteristics between each fluid. Resulting trends and observations are discussed. A linear regression methodology and results are presented in closed-form equations for the friction coefficient. Chapter 4 summarizes the work

performed in this study and summarizes the traction test results, draws major conclusions, and recommends future work which could be done to further enhance the tribology field.

CHAPTER 2

EXPERIMENTAL TEST METHODOLOGY

2.1 Introduction

In this chapter, the major components and pertinent measurement systems of the high-speed, two-disk tribometer are described. Details of the test methodology for the traction tests performed in Chapter 3 are outlined. The last section describes inspection equipment and procedures completed for disk specimens used in the traction tests for this study.

2.2 Main Operating Principle of the Two-Disk Test Set-up

The two-disk test machine used in this study is shown in Figure 2.1, while a top view schematic is shown in Figure 2.2. The test machine was developed to emulate aerospace and automotive operating conditions through tightly controlled experiments by loading a pair of rotating disks against each over a wide range of speeds, Hertzian contact

Figure 2.1: An image of the high-speed, two-disk tribometer used to conduct traction tests. Adapted from Ref. [7].

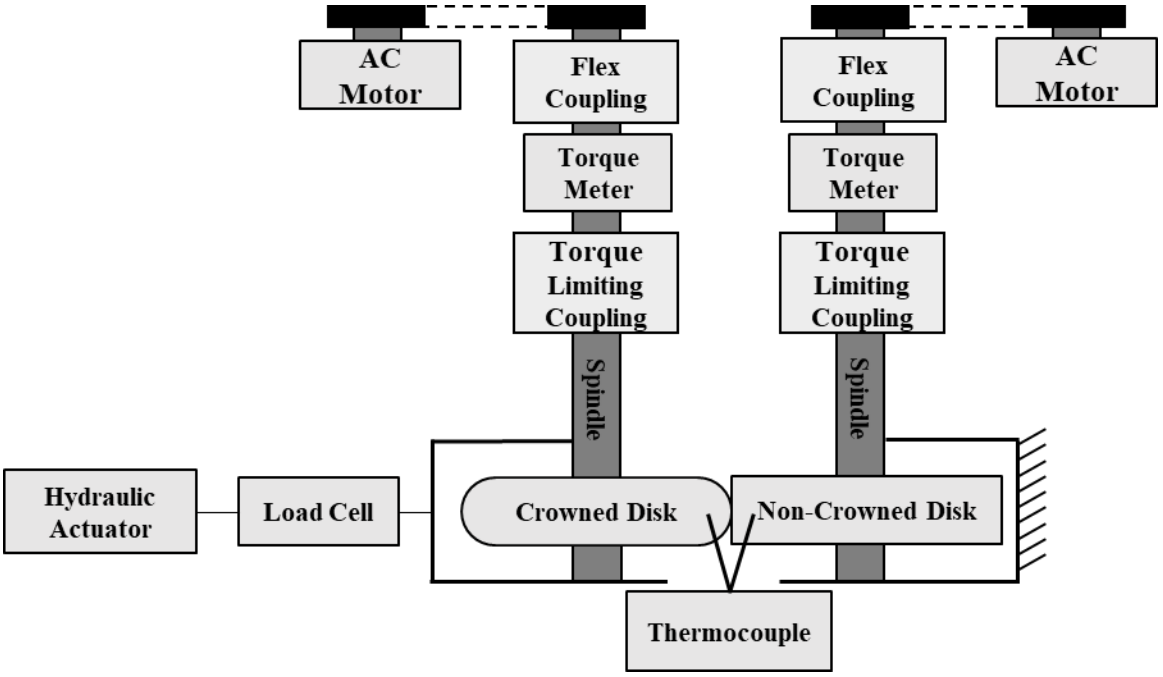

Figure 2.2: Top view schematic of the two-disk tribometer with major components illustrated.

pressures (σ_{Hertzian}), and lubricant temperatures (θ_{lube}). Only the most relevant components of this set-up will be described here while complete details can be found in Handschuh et al. [7].

Rotational speeds for disk specimens were controlled independently by an Allen Bradley PowerFlex 755 Variable frequency drive, which controlled two 50 HP AC motors. Each disk i ($i=1,2$) could be rotated up to a speed of $\Omega_i = 10,000$ rpm using a V-belt speed increaser. Since the speed of each disk was controlled independently, wide ranges of surface velocities u_i were possible, defined as

$$u_i = \frac{2\pi}{60} r_i \Omega_i \,, \tag{2.1}$$

where r_i is the radius of each disk. With the radii used for the specimens, it was possible to achieve a maximum surface velocity of 56.5 m/s for each disk. Under the general conditions of a contact that is subjected to combined rolling and sliding, surface velocities are of the disks are not equal, $u_1 \neq u_2$. As such, two composite speed parameters are used to define the speed conditions of the contact. One is the average of the two surface velocities, known as rolling (entrainment) velocity in the field of tribology, defined as

$$u_r = \frac{u_1 + u_2}{2} \,. \tag{2.2}$$

The other is sliding velocity, representing the differential of surface speeds as

$$u_s = u_1 - u_2 \,. \tag{2.3a}$$

A dimensionless parameter, called slide-to-roll ratio, can be defined to characterize the level of sliding in of the contact. It is defined as

$$SR = \frac{u_s}{u_r} = \frac{2(u_1 - u_2)}{u_1 + u_2}. \tag{2.3b}$$

The current set-up with the stated surface velocity ranges is capable of achieving a maximum rolling velocity of $u_r = 56.2$ m/s under pure rolling conditions (i.e. $u_s = 0$, $SR = 0$) and $u_r = \pm 37.7$ m/s at $SR = \pm 1.0$ ($u_s = \pm 37.7$ m/s). The operating limits of u_r and u_s are plotted in Figure 2.3 as a function of *SR*.

The loading mechanism was a linear, hydraulic actuator, which thrusted the left disk into the right disk with forces up to $F = 10$ kN. The actuator consisted of two ports: one each for piston retraction and extension, which were regulated by a proportioning valve to maintain the desired normal force using feedback from an inline load cell. The relationship between contact normal force *F* and the corresponding maximum Hertzian contact stress σ_{Hertzian} is shown in Figure 2.4 for the disks used in this study.

Two 3-kW electric sump heaters were used to maintain a user-defined lubricant inlet temperature up to 160ºC. A 1-HP pump could distribute lubrication at a rate of 0.5 1/min through four 0.2 mm diameter nozzle outlet ports. The nozzle exit velocity was chosen to replicate the counterparts in high-speed gearboxes where dip lubrication cannot be adopted.

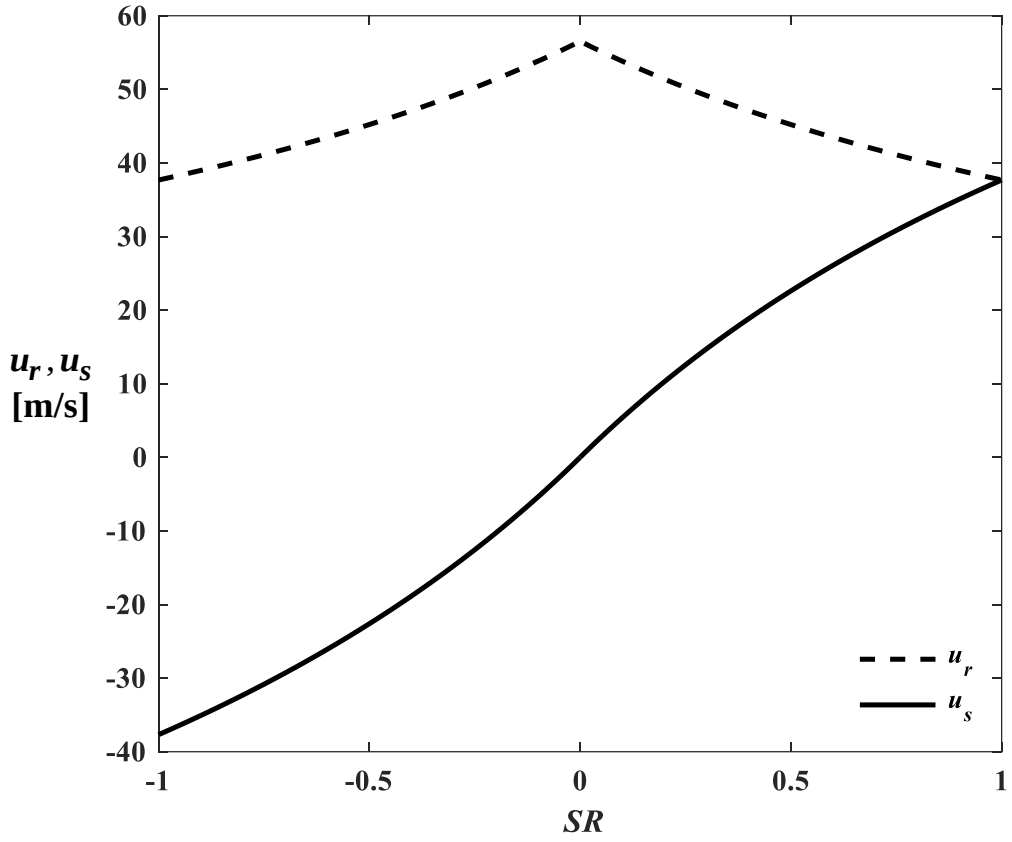

Figure 2.3: Machine operating limits for u_r and u_s over $-1 \leq SR \leq 1$ for the disks used in this study.

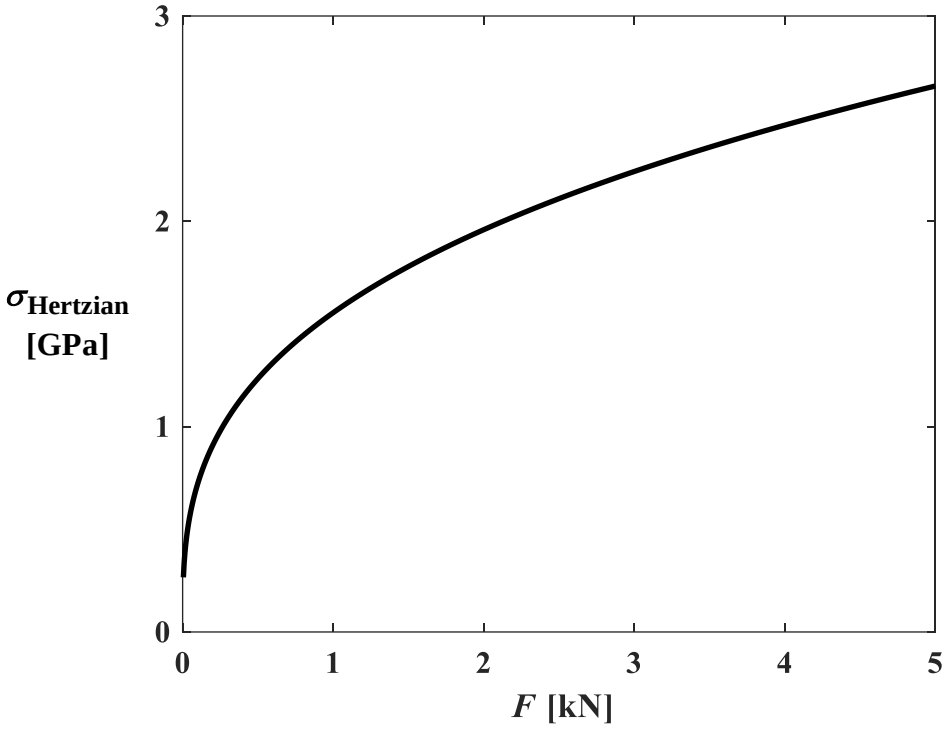

Figure 2.4: Relationship between σ_{Hertzian} and F for disks used in this study.

2.3 Measurement Systems and Sensors

As in any tribometer, the focus in a two-disk test set-up is to measure friction and temperature conditions of the lubricated contact that is under combined rolling and sliding actions. For determining the traction or friction taking place at the contact interface, levels of torque provided to each disk by the drives must be measured accurately. As shown in Figure 2.2, this was done through dedicated torque-meters placed on both disk spindles. Both inline toque-meters were rated to maximum torque of 56.5 Nm and had an accuracy of 0.0565 Nm, (or 0.1% full-scale) which was deemed sufficient for traction measurements. Torque limiting couplings were placed between the torque meters and disks for hardware protection as scuffing failures may cause a very large and rapid increase in contact torque.

Figure 2.5 shows a free-body diagram of both spindle assemblies when the roller pair is loaded by a normal load *F* and $u_1 < u_2$. The torque measured by each torque meter are given as T_1 and T_2. Here, if there were no other external torque applied on the spindles, T_1 and T_2 would be equal in magnitude and would represent the traction torques $T_{f,1} = r_1 F_f$ and $T_{f,2} = r_2 F_f$ caused by the friction force F_f. However, as shown in Figure 2.5, each spindle is subjected to other external torques representing the rolling element bearing torque losses (depicted as $\sum T_{b,i}$ in Figure 2.5) and losses due to windage and churning of the disks in the fluid-air media ($T_{s,i}$). As a result, T_1 and T_2 are not equal as shown in Figure 6(a) through an example traction test. Therefore, they cannot be used directly to determine the tractions torque. Handschuh et al. [7] presented a detailed

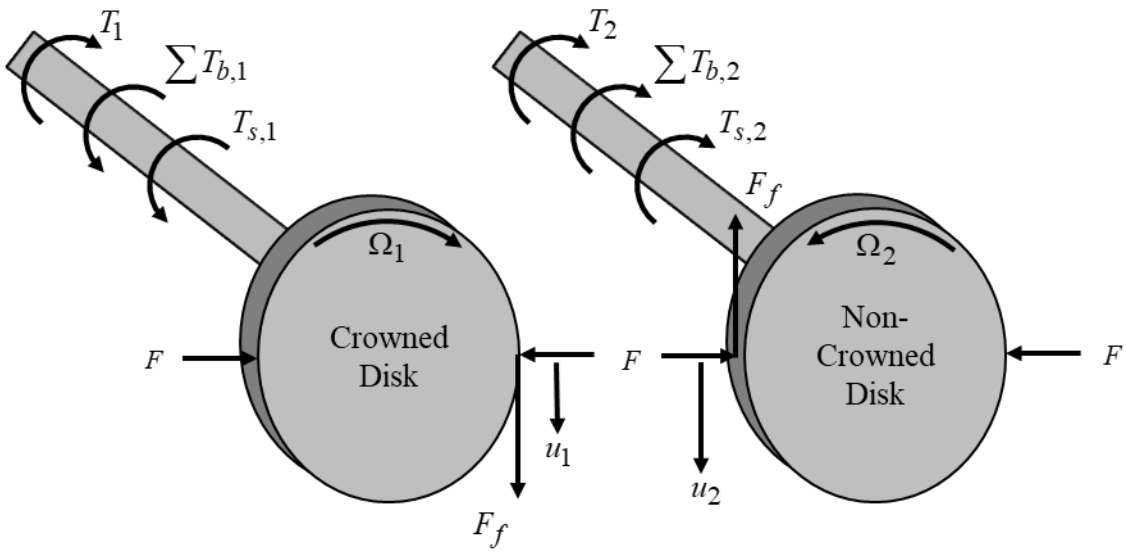

Figure 2.5: Free-body diagram of disk-spindle assembly assuming $u_2 \geq u_1$.

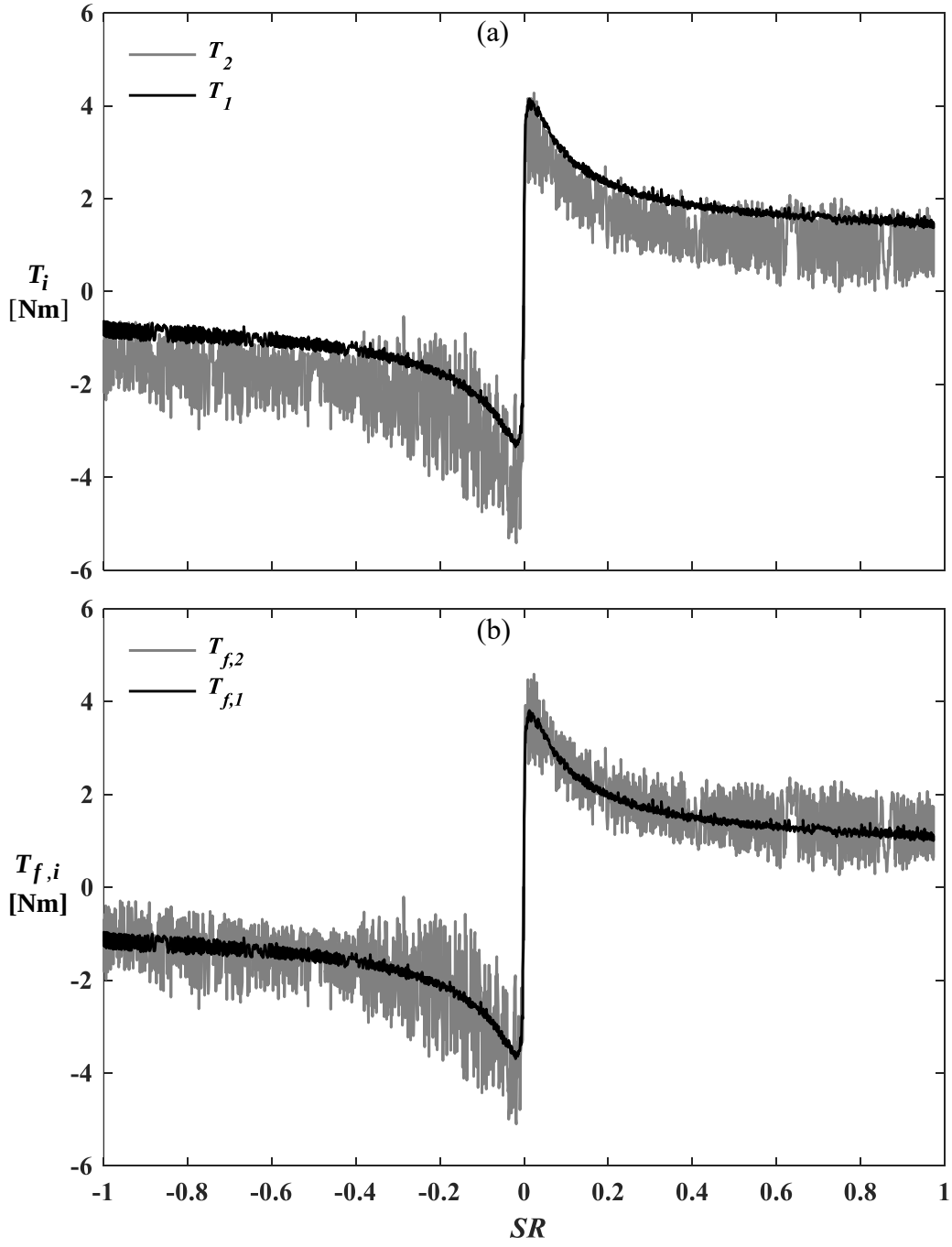

Figure 2.6: A set of measured torques (a) with drag and spin losses present, and (b) with drag and spin losses removed.

procedure on how to remove these torque losses from T_1 and T_2. For this, a set of experiments were conducted at pure rolling conditions (i.e. $u_1 = u_2$ or $SR = 0$) at various F and u_r levels as this pure rolling condition should represent zero traction torque T_c ($T_{f,1} = T_{f,2} = T_c = 0$), leaving only the other torques to form T_1 and T_2. The data under purely rolling conditions were surface-fit to remove $\sum T_{b,i}$ and $T_{s,i}$ from T_i to isolate $T_{f,1} = T_{f,2} = T_c = r_i F_f$ [7]. Figure 2.6(b) presents the same data in Figure 2.6(a) with all $\sum T_{b,i}$ and $T_{s,i}$ removed such that what remains can be called $T_{f,1}$ and $T_{f,2}$, that are shown to be equal to each other.

A ± 13.3 kN load cell was placed between the driven side bearing housing and the output shaft of the hydraulic actuator to measure the applied normal force *F* produced by the hydraulic actuator. This measurement is essential, along with applicable material properties and geometry of each disk for determining the maximum Hertzian contact pressure (σ_{Hertzian}) of the contact. Using the load cell and torque-meter measurements in tandem, along with the above removal process, the overall coefficient of friction for the contact is found as:

$$\mu = \frac{F_f}{F} = \frac{T_c / r_i}{F}. \tag{2.4}$$

The surface bulk temperatures $\theta_{b,i}$ ($i = 1, 2$) are a critical measurement when evaluating traction data. Recording accurate surface bulk temperatures can be difficult due to how contact type thermocouples are spring loaded against the contact surface, which

cause additional heat generation due to friction. To mitigate additional heat generation and ensure accurate temperature readings, the type K contact thermocouples were held in place by fixtures. The fixtures were positioned so the probes were gently loaded in the center of contact area for each disk to maintain constant contact with the disks without generating excess heat.

2.4 Traction Test Procedure and Test Matrix

A set of automotive traction tests will be performed in this study using super-finished disks made of an automotive gear steel to experimentally determine the friction characteristics for three different automotive transmission fluids. Overall disk dimensions and material properties are shown in Figure 2.7 and Table 2.1, respectively. In each traction test, SR was varied linearly from -1 to $+1$ by varying u_1 and u_2 in unison while maintaining a constant u_r, F, and θ_{lube}. Since the disks in this study had the same radius ($r_1 = r_2$), $3u_1 = u_2$ at $SR = -1$ and $u_1 = 3u_2$ at $SR = 1$ while $u_1 = u_2$ at $SR = 0$, indicating that u_1 was increased linearly at the same rate that u_2 was reduced linearly. The faster disk was exactly three times faster than the slower disk at $SR = \pm 1$. These synchronized linear surface velocity changes defining a traction test at $u_r = 20$ m/s are shown in Figure 2.8.

A total of 36 tests at unique combinations of u_r, θ_{lube}, and F were performed for each transmission fluid type. Four F increments were used, ranging between $F = 500$ to

4,400 N, corresponding to a σ_{Hertzian} range of 1.2 to 2.5 GPa. Three separate u_r values

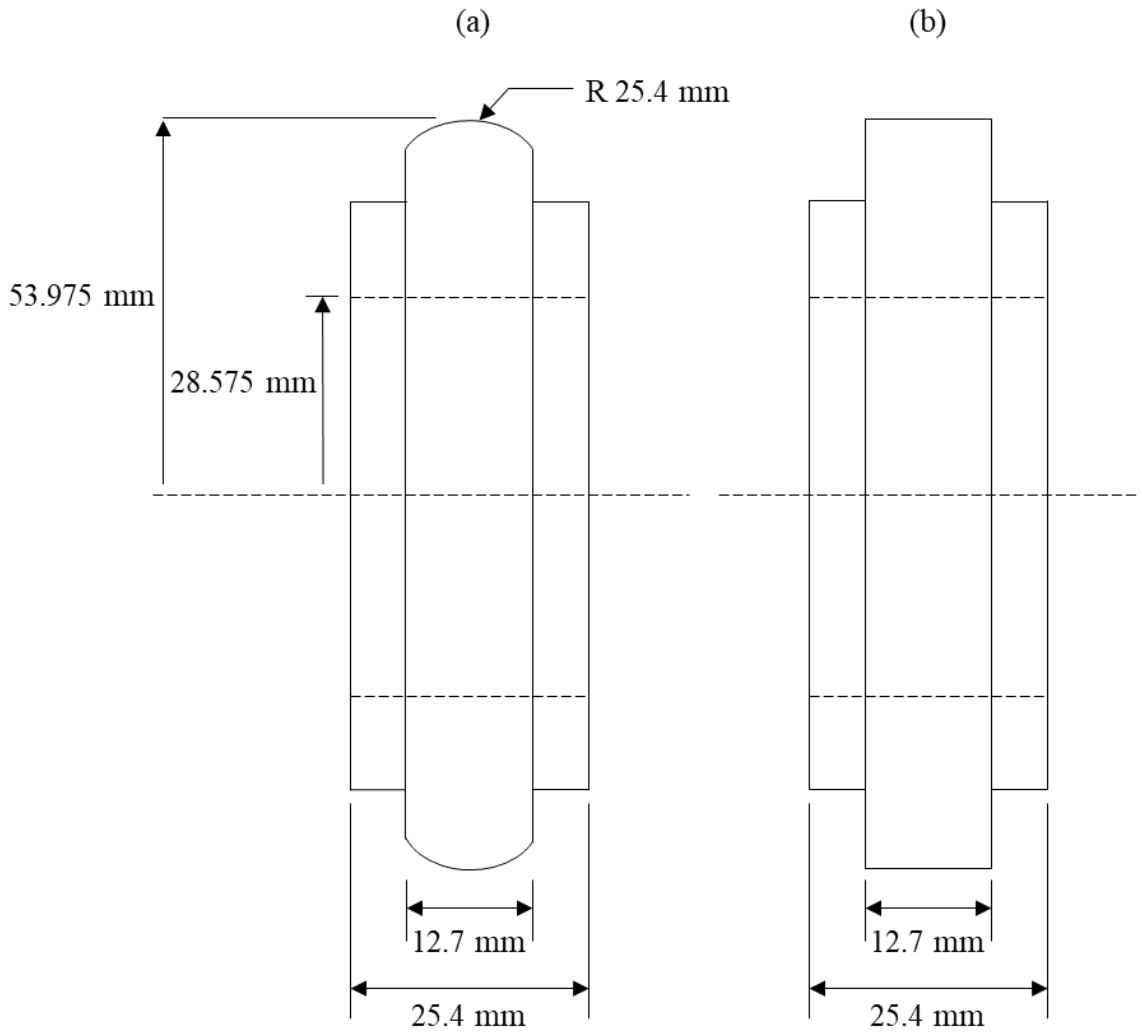

Figure 2.7: Overall dimensions of (a) crowned and (b) non-crowned disk specimens.

Table 2.1: Material properties data for disk specimens.

Property	Unit	Symbol	Value
Density	$\mathrm{kg/m^3}$	ρ_i	7850
Poisson's Ratio	--	ν_i	0.3
Modulus of Elasticity	GPa	E_i	210
Thermal Conductivity	W/m/K	k_i	44.5
Specific Heat	J/kg/K	c_i	470

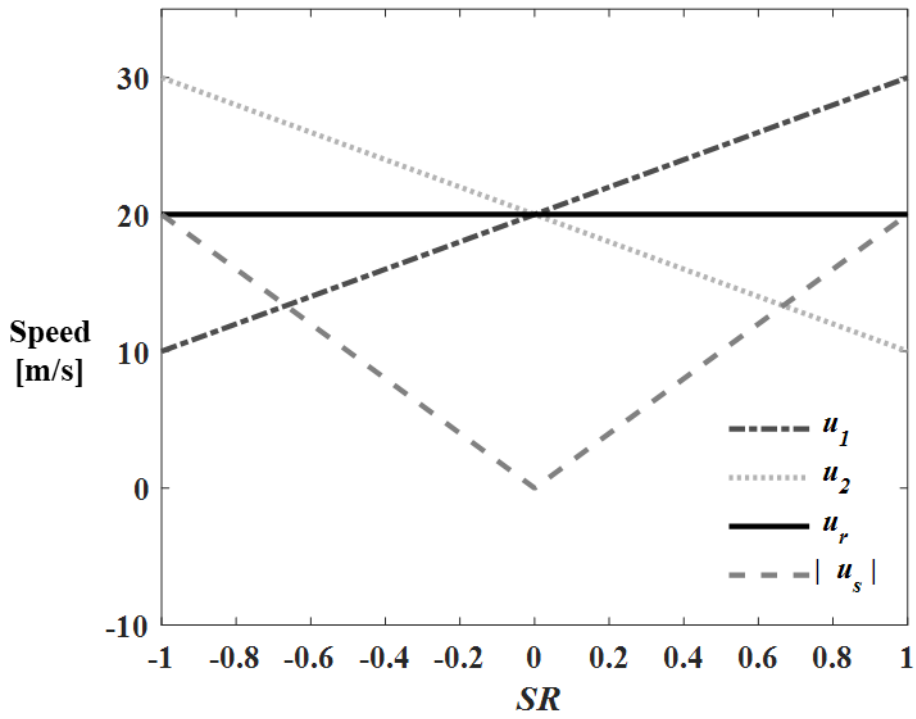

Figure 2.8: Disk surface speeds during a traction test when $u_r = 20$ m/s for the geometry used in this study.

of 10, 20 and 30 m/s and θ_{lube} values of 40, 70 and 90ºC were tested. The full traction test matrix executed in this study is defined in Table 2.2.

2.5 Inspection Procedures and Parameters

All disk specimens were inspected before and after all traction tests concluded (i) by measuring the surface roughness at three equally spaced positions in both the circumferential and axial directions by a contact profilometer, (ii) by taking topographical non-contact surface measurements with an optical profiler, and (iii) by capturing microscopic and macroscopic digital images of the contact surface. Each disk pair was subjected to 36 unique traction tests, each lasting 10 min, and to torque removal experiments described in Section 2.3. As such, the total test time for each disk pair was about 10 hours. Since the disks were chemically processed post manufacturing to achieve very smooth surfaces, changes in surface roughness of each steel disk were expected to be insignificant. This was confirmed through pre and post-test roughness measurements. A Taylor Hobson Form Taylsurf-120 was used for the contact-type surface roughness measurements. Figure 2.9(a) and shows the surface roughness profile for a super-finished disk used in this study and (b) an axially grounded surface disk of the same automotive grade steel. Standard ISO cutoffs were used for the expected roughness range, with the upper cutoff being 0.25 mm and lower cutoff 0.0025 mm, respectively. The data length was set to 1.27 mm. The super-finished disk was almost an order of magnitude smoother than a typical axially grounded disk. The surface roughness was expected to vary slightly within the contact zone. Careful consideration was taken to make sure each disk was arranged to be measured at this location in a consistent manner.

Table 2.2: Test matrix for traction tests of Chapter 3.

Lubricant	*SR*	θ_{lube} [˚C]	u_r [m/s]	$\sigma_{Hertzian}$ [GPa]
A, B, C	-1 to 1	40	10	1.2, 1.9, 2.3, 2.5
			20	1.2, 1.9, 2.3, 2.5
			30	1.2, 1.9, 2.3, 2.5
		70	10	1.2, 1.9, 2.3, 2.5
			20	1.2, 1.9, 2.3, 2.5
			30	1.2, 1.9, 2.3, 2.5
		90	10	1.2, 1.9, 2.3, 2.5
			20	1.2, 1.9, 2.3, 2.5
			30	1.2, 1.9, 2.3, 2.5

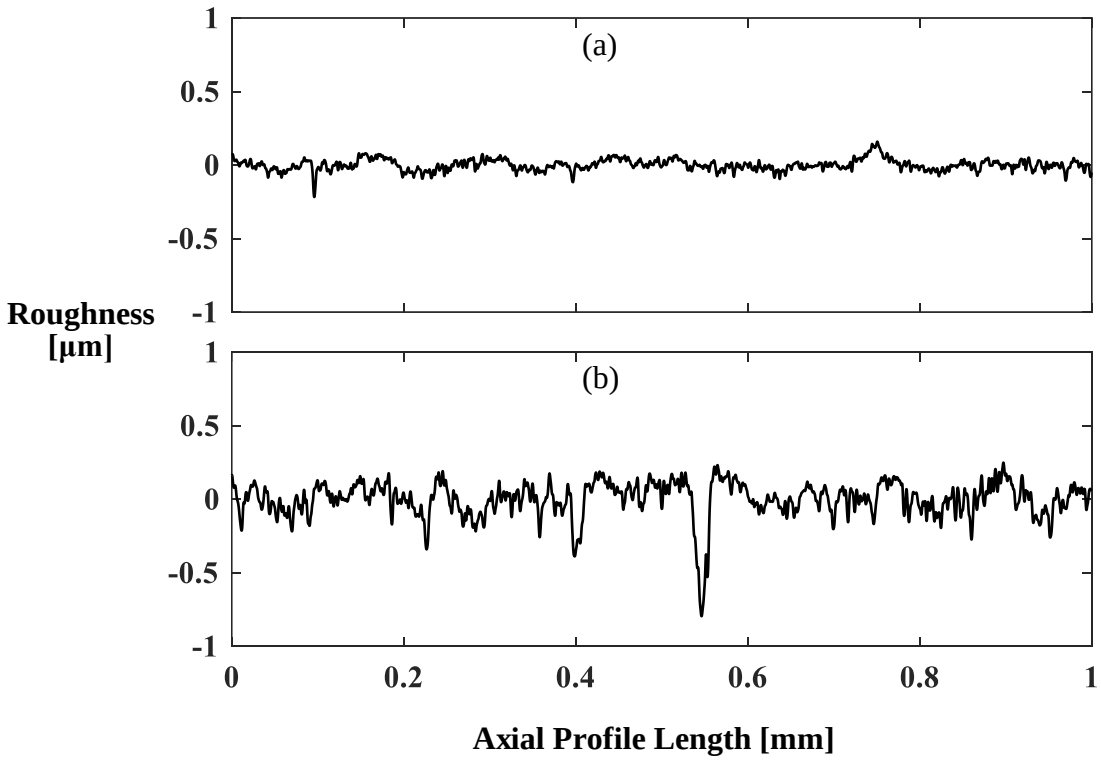

Figure 2.9: Example of measured surface roughness profiles for (a) a super-finished disk used in this study and (b) an axially ground disk surface of the same material.

3D surface profiles were measured with a ZYGO ZeGage^{TM}. This device was capable of nanometer precision, with a resolution of 1.9 million pixels in a single image. An example disk surface roughness map is shown in Figure 2.10. A high pass-filter was employed to remove form and waviness. Field stitching was enabled on the device to examine a 3.5 x 3.5 mm area that fully enveloped the center region of each disk where contact occurred. This resulted in a 3x3 stitched grid with overlapped boarders to obtain a smooth and continuous measurement.

Microscopic and Macroscopic digital images of the disk specimens were captured with a Keyence VHX – 950F. Macroscopic images were recorded at 20x magnification, while microscopic images were recorded at 100x magnification. Caution was taken to not distort images by maintaining the same camera settings and disk position for all images. An example (a) microscopic and (b) macroscopic image of a flat disk is shown in Figure 2.11.

2.6 Summary

In this chapter, a high-speed, two-disk tribometer has been introduced. The corresponding disk specimens and associated kinematics used to perform traction tests were described. Key measurement systems and procedures were presented including how to obtain the traction torque and how to perform traction tests. A test matrix to be implemented in the next chapter was also specified.

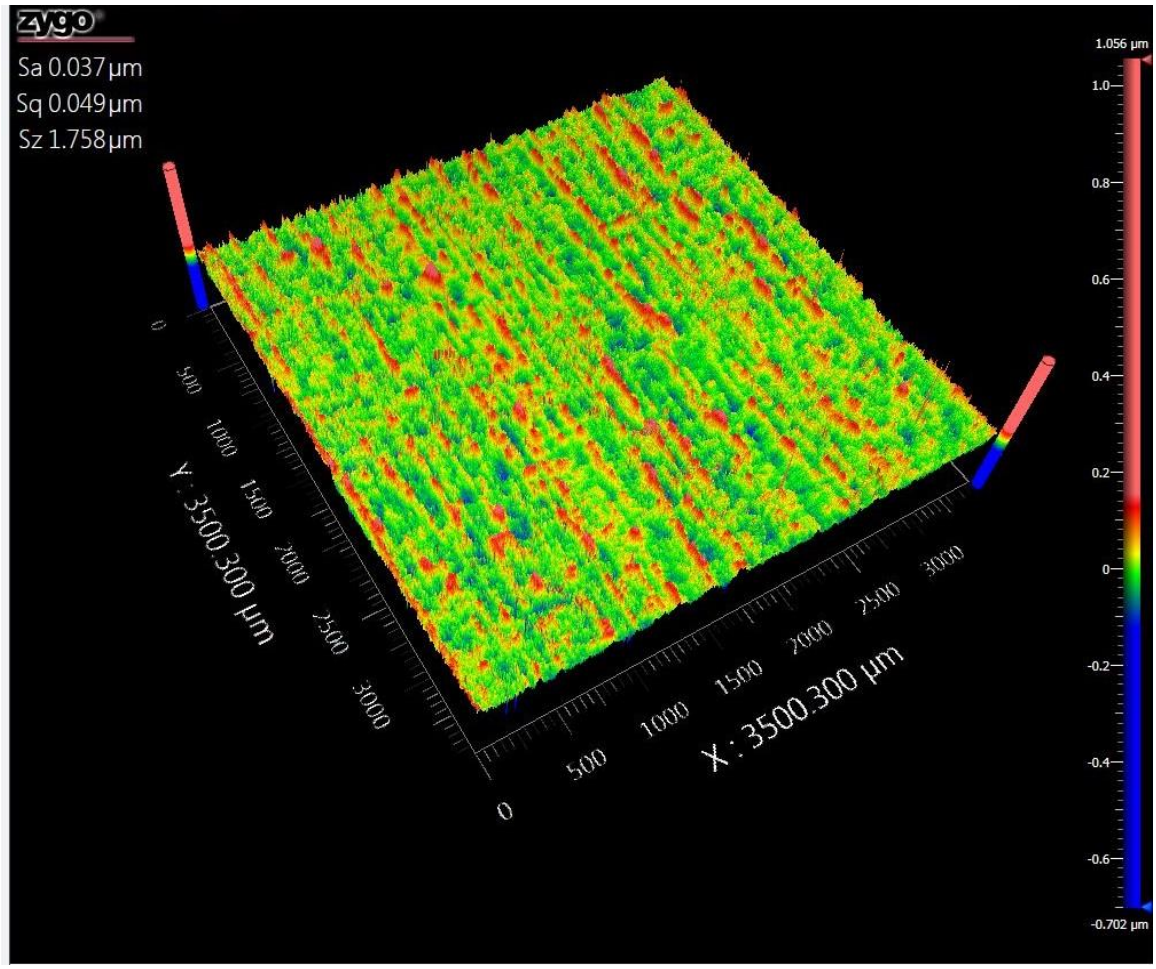

Figure 2.10: A surface roughness map of a super-finished disk used in a traction test.

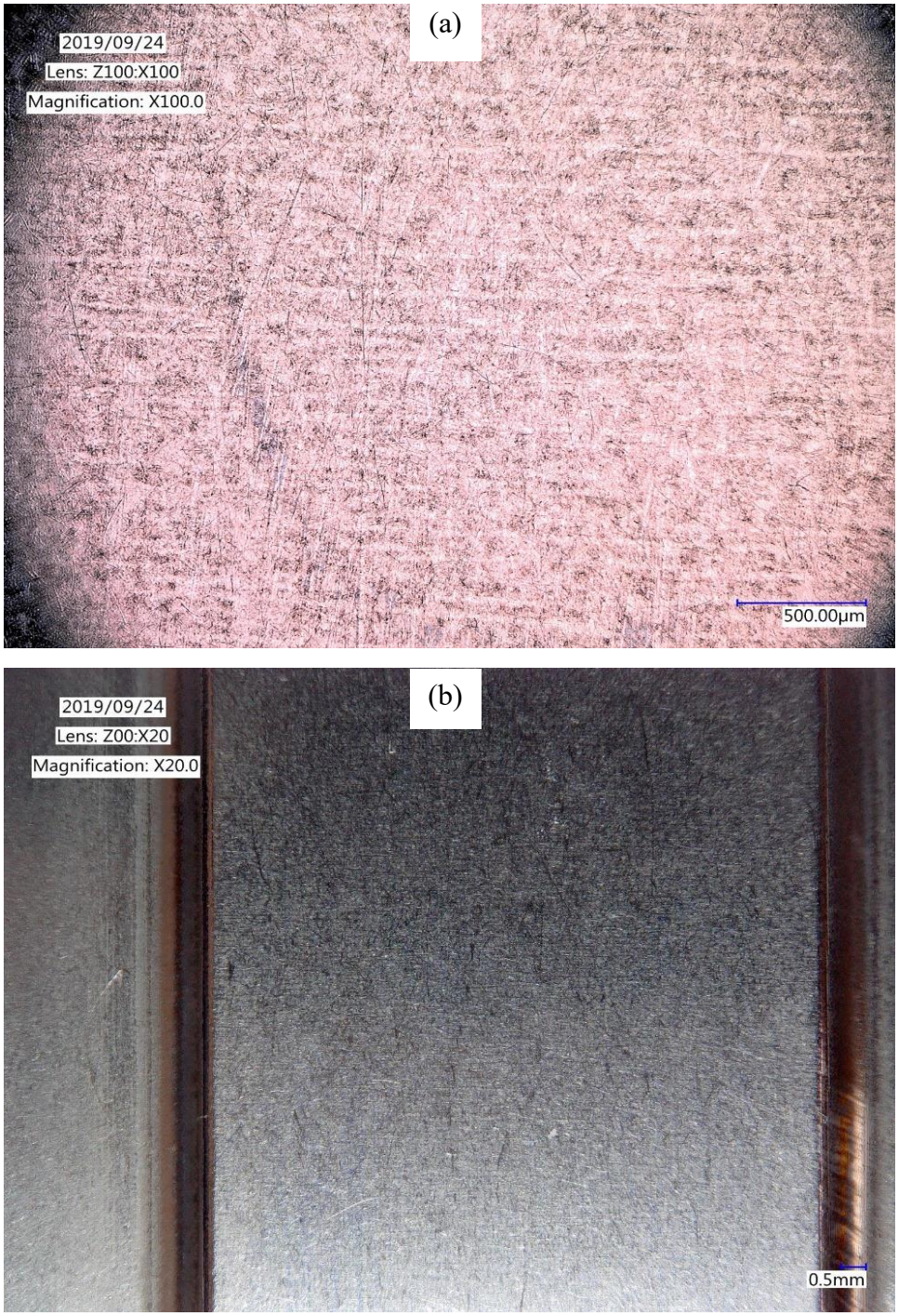

Figure 2.11: Examples of (a) microscopic and (b) macroscopic images of a flat disk used in this study.

CHAPTER 3

TRACTION MEASUREMENT RESULTS

3.1 Introduction

This chapter presents the measurement results from the traction experiments performed in accordance with the test matrix defined in Table 2.2. Traction curves taken at representative speed, temperature, and load combinations are presented for each lubricant. Experiments performed to demonstrate the repeatability of the test methodology and the set-up are presented. Asymmetry observed in the traction curves with respect to the sliding ratio is described. Comparisons between three lubricants tested are made at various operating conditions. The subsequent sections describe the methodology used to perform an ordinary least-square linear regression of the measured traction curves to obtain closed-form empirical formulae for traction torque T_c as a function of σ_{Hertzian}, u_r, η, and SR.

3.2 Experimental Results

One critical metric for evaluating the performance of lubricants is their coefficient of friction μ, which is crucial in accessing the frictional power losses of gear mesh interfaces. μ can be derived directly from measured contact torque T_c using Eq. (2.4). The test matrix shown in Table 2.2 outlines a wide variety of operating conditions that includes three automotive transmission fluids operating at high speeds to evaluate their friction characteristics. To provide a direct comparison, all three lubricants were tested under the same conditions.

The traction curves shown in the proceeding sections present T_c versus slide-to-roll ratio SR as shown in Figure 3.1. It was observed that T_c depends significantly on SR. The magnitude of measured contact torque $|T_c|$ is approximately zero when $SR = 0$ as a result of no sliding friction. $|T_c|$ increases sharply as $|SR|$ increases slightly from zero, reaching a maximum value when *SR* is rather small, $|SR| \approx 0.05$ in this case, after which decaying with increasing *SR*.

3.2.1 Measurement Repeatability

Test repeatability is paramount in any experimental study. Experiments were conducted to access the variance in measured contact torque T_c to ensure consistent results over varying operating conditions and machine tear down and reassembly. Figure 3.2 shows repeated traction experiments performed with lubricant B under two different operating speeds and four load conditions. The two sets of tests are very close indicating

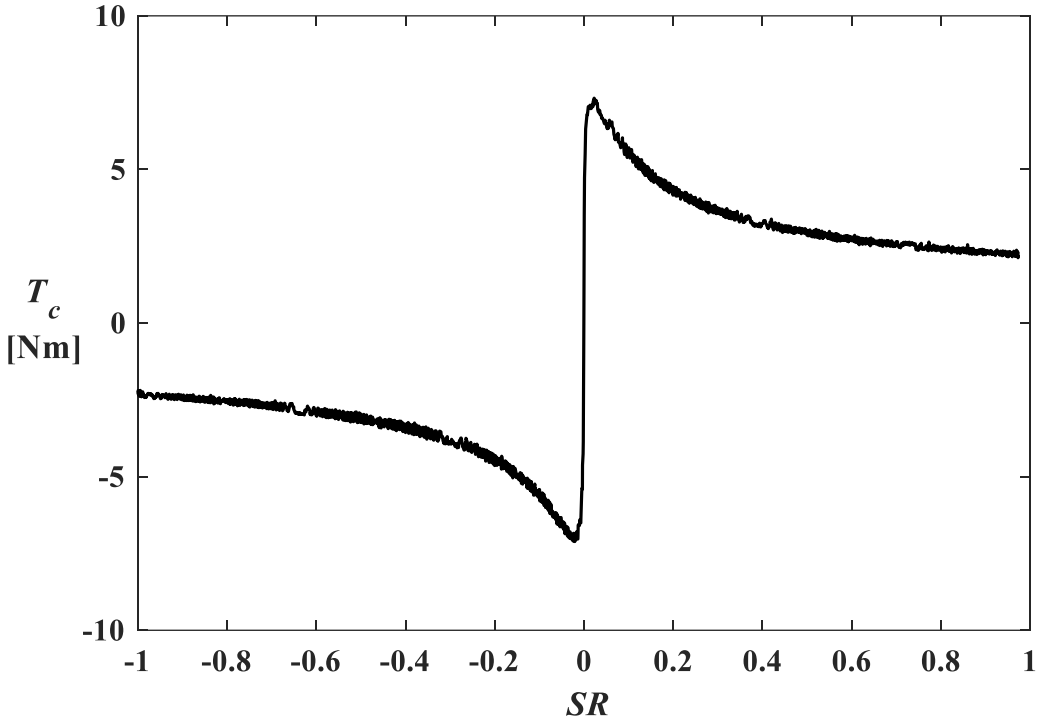

Figure 3.1: A typical measured traction curve.

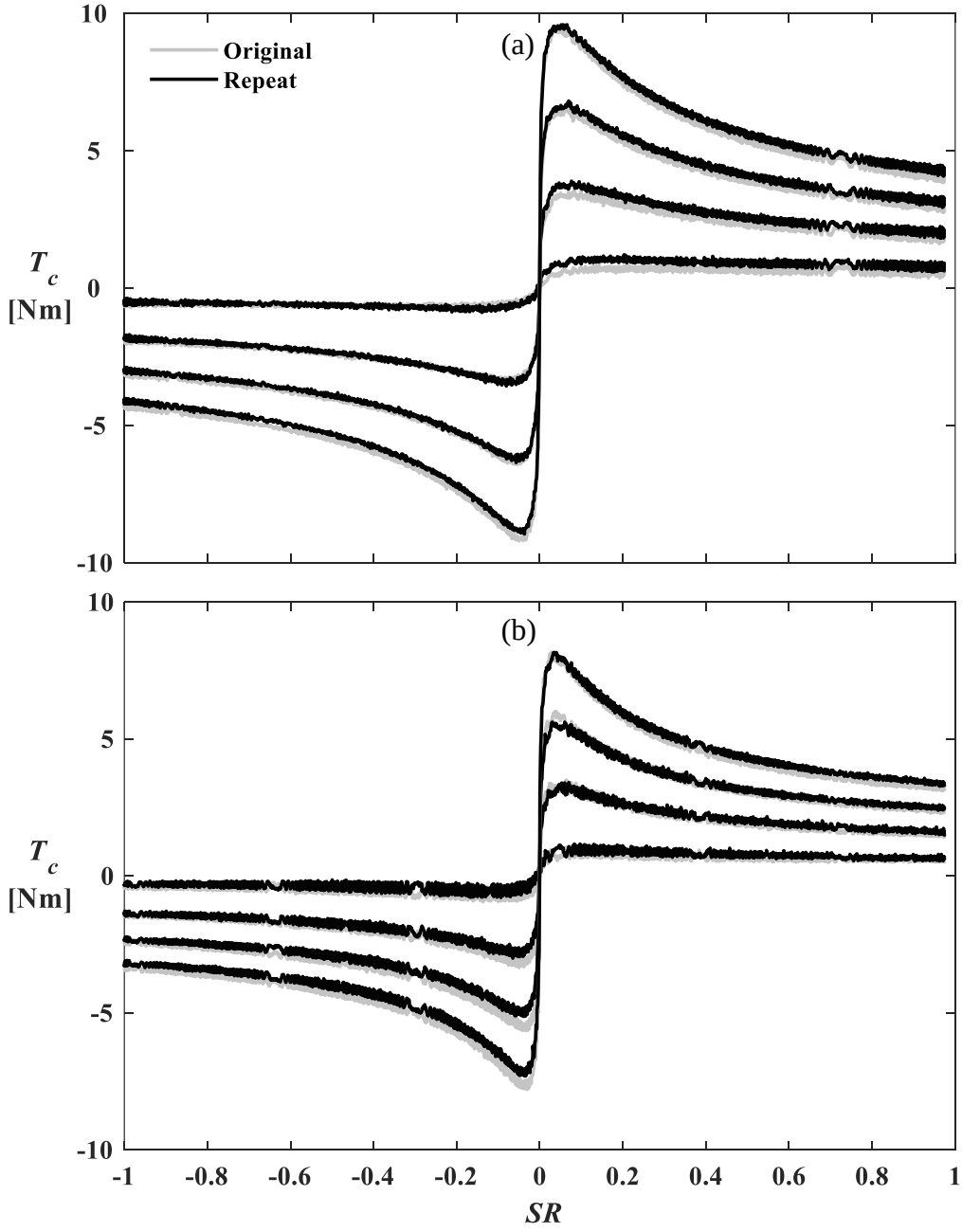

Figure 3.2: Repeatability at four normal force *F* levels using Lubricant B at (a) $u_r = 10$ m/s and (b) $u_r = 20$ m/s and $\theta_{\text{lube}} = 90°\text{C}$.

that the methodology used to measure traction torque is indeed repeatable and consistent.

3.2.2 Measured Traction Curve Asymmetry

After the torque removal procedure described in Section 2.3 was completed, the traction curves were still slightly asymmetric about $SR = 0$. Away from $SR = 0$, $|T_C|$ was most often lower in the positive SR region compared to its corresponding $-SR$ value. This difference is highlighted in Figure 3.3 for each lubricant along with accompanying measured surface bulk temperature $\theta_{b,i}$. The asymmetry was likely a result of how the tests were performed. Each traction experiment started at the highest negative sliding condition of $SR = -1$. The high sliding speed caused $\theta_{b,i}$ to increase initially but soon decrease as the sliding speed decreased until $SR = 0$. For $SR > 0$, the disks begin to heat up steadily as u_s continues to increase, reaching a maximum surface bulk temperature $\theta_{b,i}$ at $SR = 1$. As shown in Figures 3.3(d,e,f), $\theta_{b,i}$ curves are not symmetric. Viscosity of the lubricant η is inversely proportional to temperature. In the fluid region, lubricant shear stress is defined generically as

$$\tau = \eta \frac{u_s}{h}, \tag{3.1}$$

where u_s is the sliding velocity and h is the lubricant film thickness. This means that *h* is also inversely proportional to temperature. However, these effects are typically less than the decrease in η, meaning that τ decreases for a rise in θ_b. Since the disks were super-

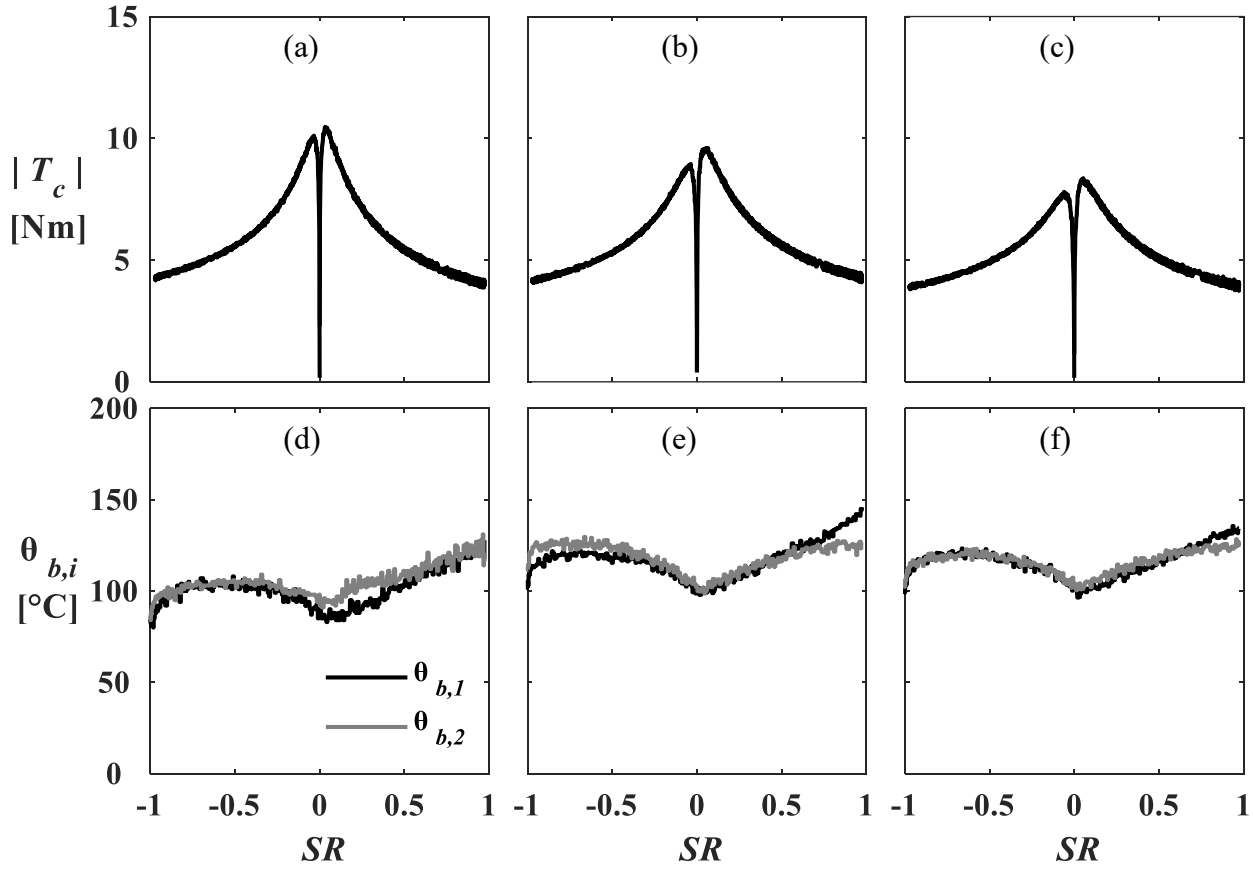

Figure 3.3: (a-c) Measured traction torque $|T_c|$ curves and (d-f) the corresponding bulk temperatures for (a,d) Lubricant A, (b,e) Lubricant B, and (c,f) Lubricant C for a traction test performed at $F = 4400\ \text{N}$, $u_r = 10\ \text{m/s}$, and $\theta_{\text{lube}} = 90\ ^\circ\text{C}$.

-finished, the reduction in h will not adversely affect the contact due to asperity interaction. Therefore, the overall τ of the contact (i.e. T_c, and hence μ) is expected to reduce, which is evident in Figure 3.3.

3.2.3 Traction Test Results

A total of 108 traction tests were performed over the various operating conditions. Only subsets of the results are presented here to feature overall observed trends and to make direct comparisons of T_c. Figures 3.4 to 3.6 show comparisons of measured T_c versus SR at various F, u_r, and θ_{lube} combinations for each lubricant. It is observed that measured T_c increases with increasing applied normal force F and decreases with increasing u_r and increasing θ_{lube}. Figures 3.7 to 3.10 show direct comparisons of measured T_c for each lubricant at $F = 1800$ and 4400 N ($\sigma_{\text{Hertzian}} = 1.9$ and 2.5 GPa), $u_r = 10$ and 30 m/s, and $\theta_{\text{lube}} = 40$ and 90 °C for a total of eight combinations for each lubricant. The corresponding coefficient of friction values is listed in Table 3.1 at $SR = 0.05,\ 0.5$ and 1.0 from the test conditions in Figures 3.7 to 3.10. The following observations can be made from Figures 3.4-3.10 and Table 3.1 in terms of friction performance of the three lubricants considered:

- At $SR = 0.05$, where T_c was a maximum, the measured friction coefficient μ values were within the ranges $[0.028, 0.054]$, $[0.026, 0.055]$ and $[0.026, 0.049]$ for Lubricants A, B, and C, respectively.

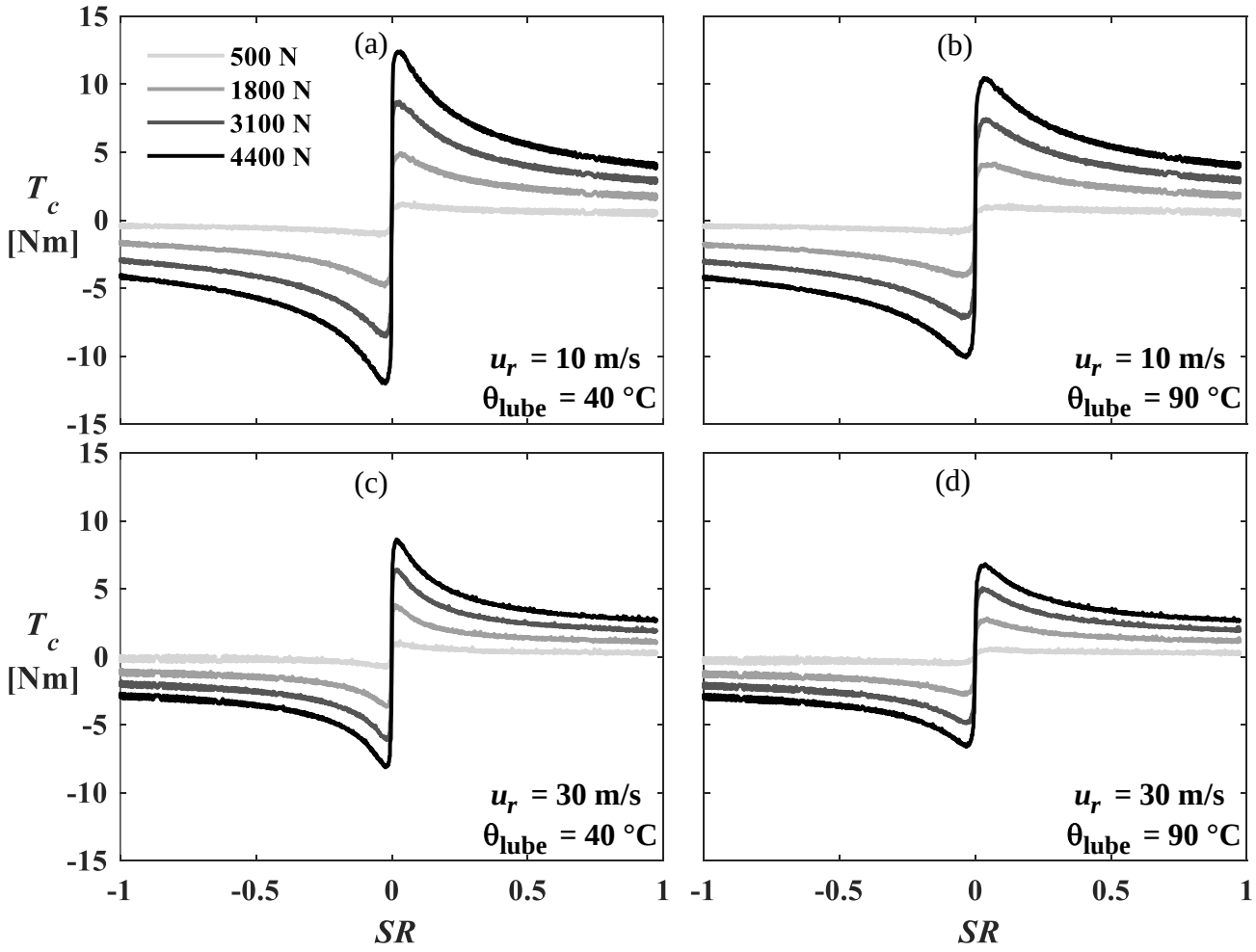

Figure 3.4: Measured T_c curves for Lubricant A at various F, u_r, and θ_{lube} values.

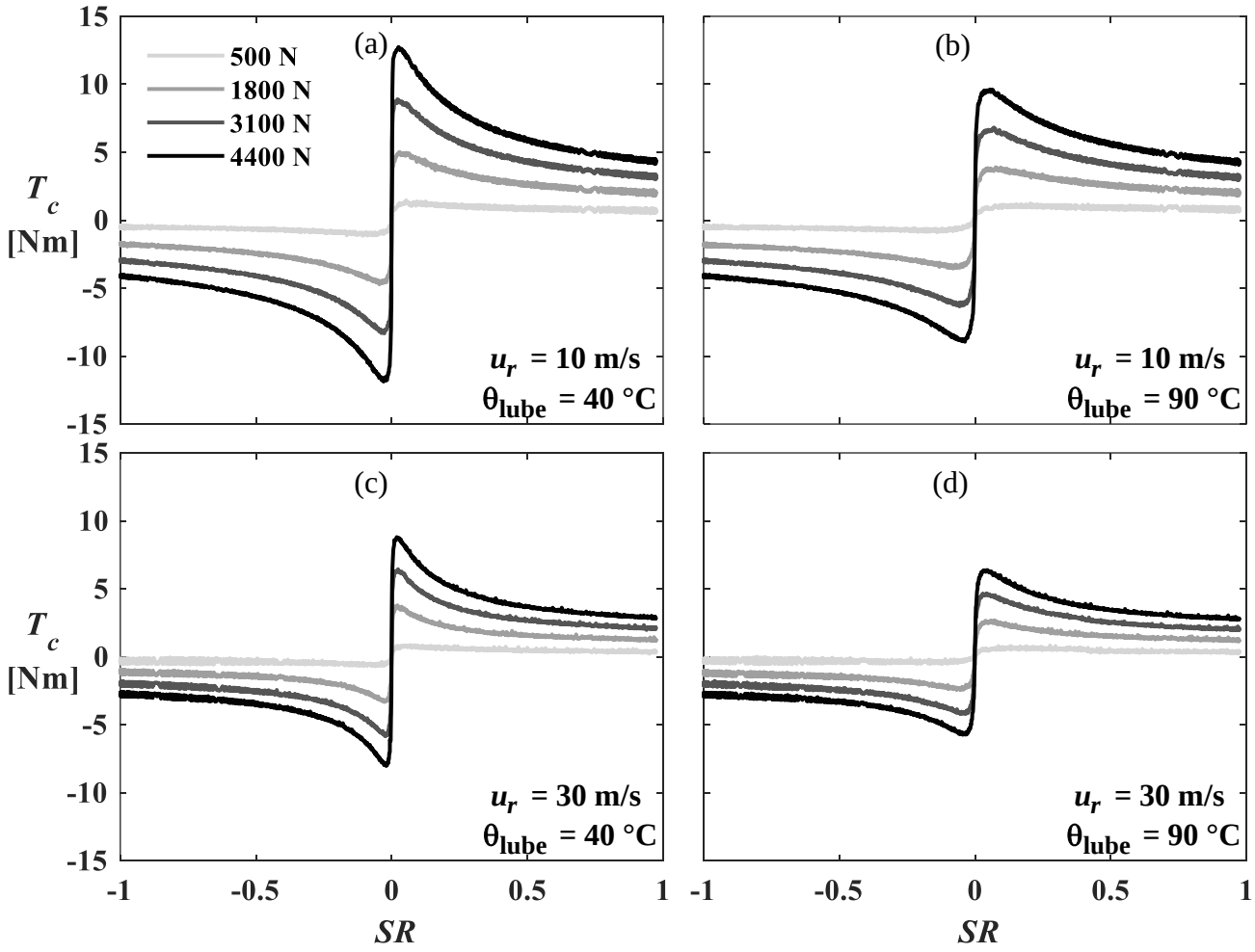

Figure 3.5: Measured T_c curves for Lubricant B at various F, u_r, and θ_{lube} values.

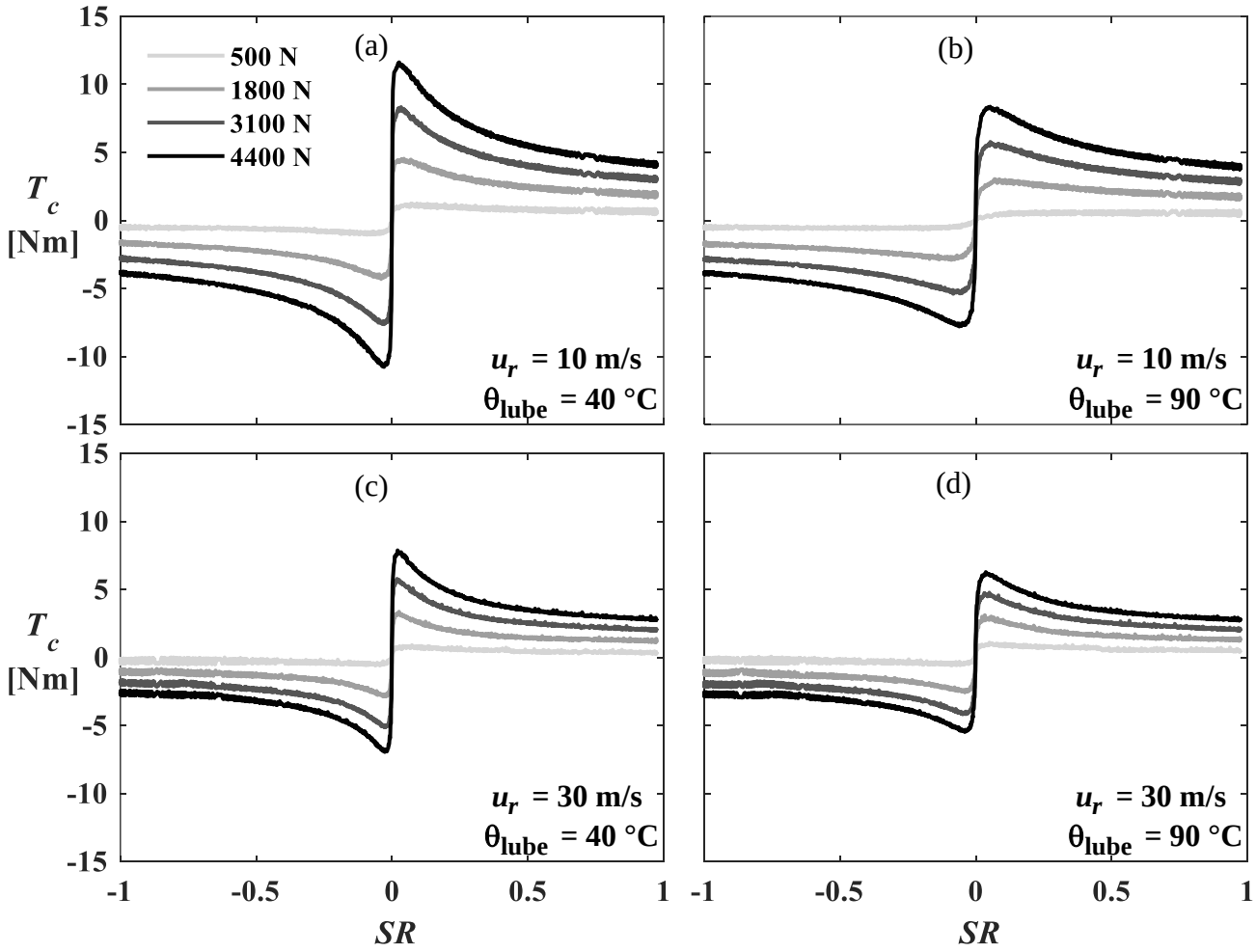

Figure 3.6: Measured T_c curves for Lubricant C at various F, u_r, and θ_{lube} values.

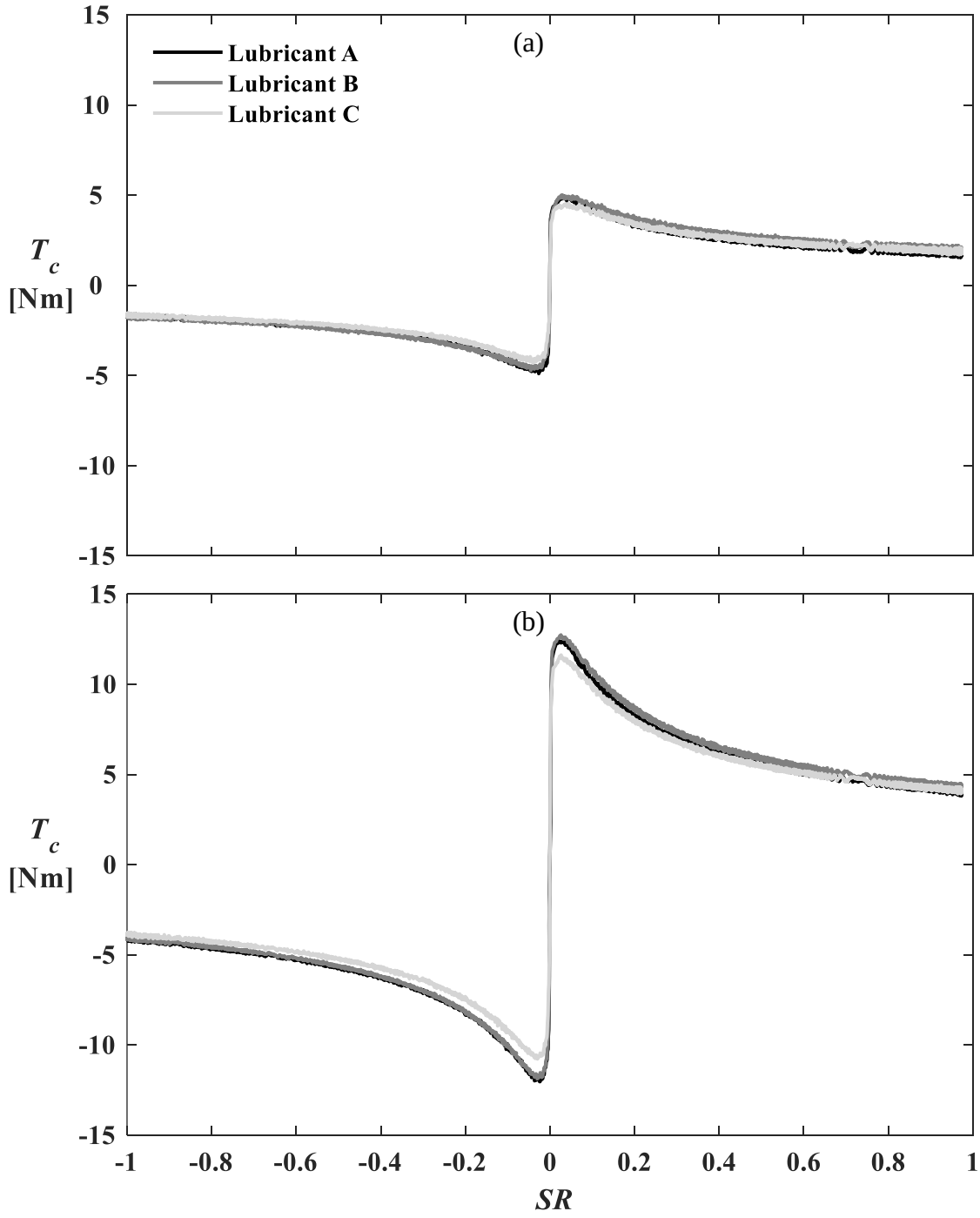

Figure 3.7: Comparison of measured T_c curves for three Lubricants at (a) $F = 1800$ N and (b) $F = 4400$ N when $u_r = 10$ m/s and $\theta_{\text{lube}} = 40$ °C .

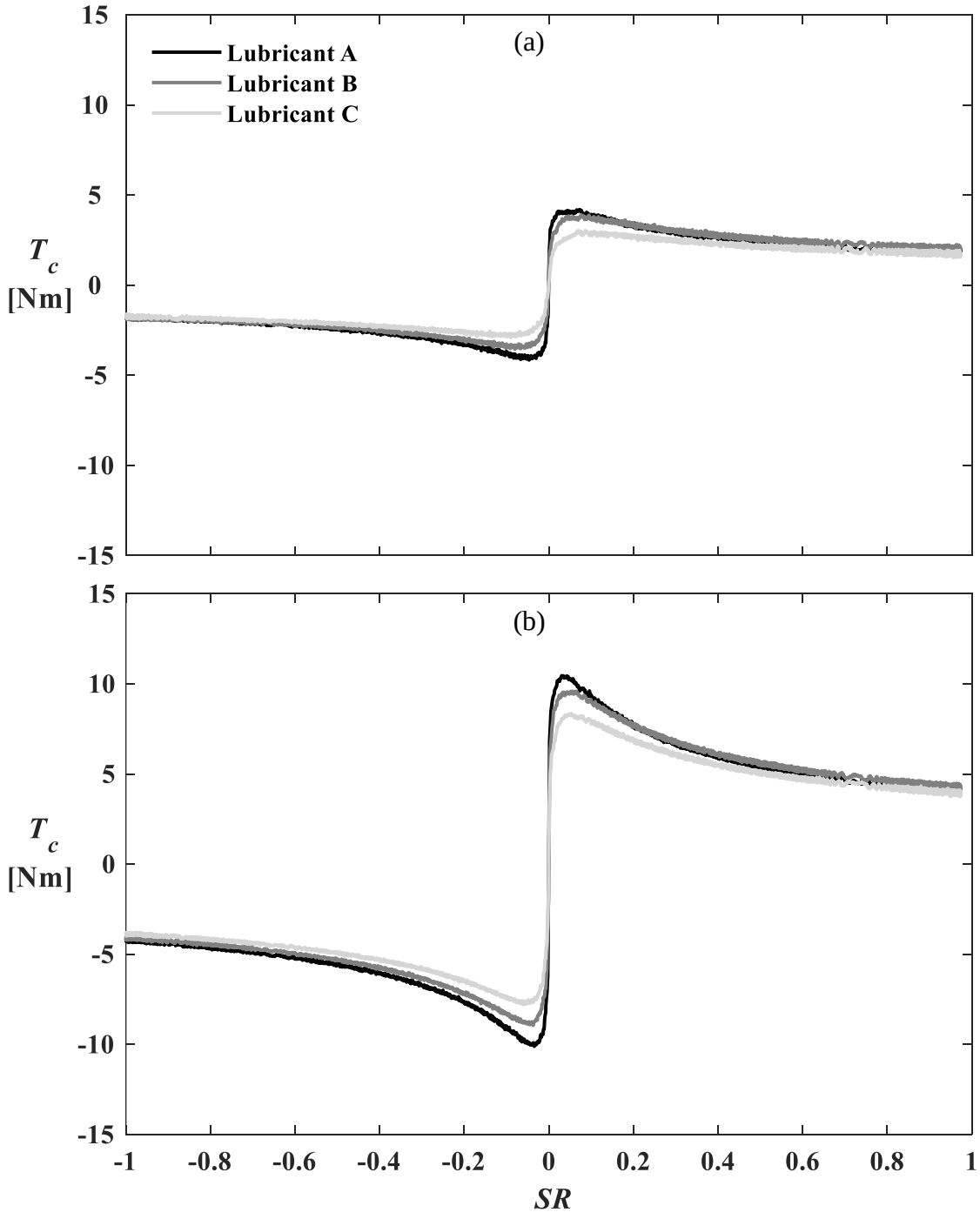

Figure 3.8: Comparison of measured T_c curves for three Lubricants at (a) $F = 1800$ N and (b) $F = 4400$ N when $u_r = 10$ m/s and $\theta_{\text{lube}} = 90$ °C.

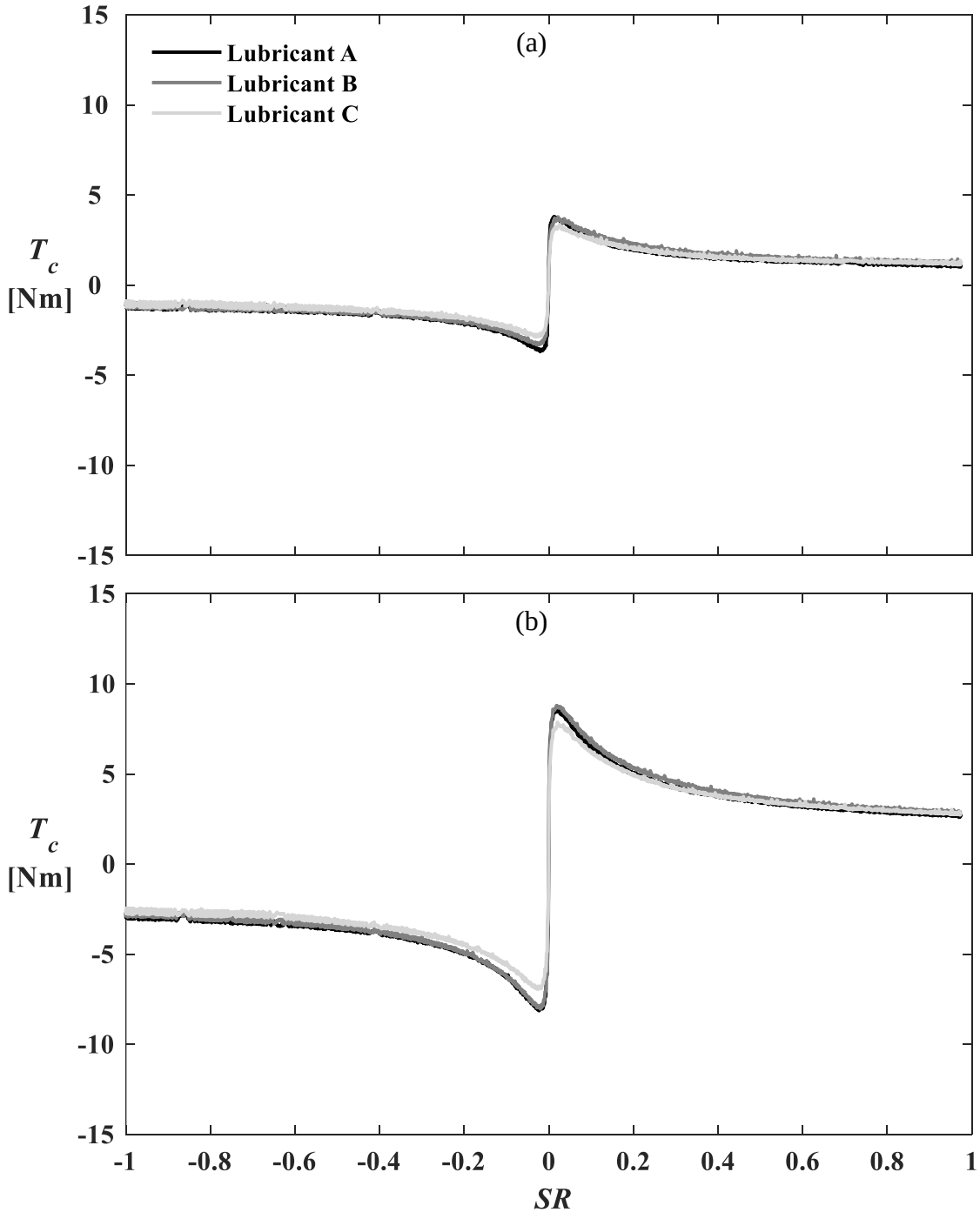

Figure 3.9: Comparison of measured T_c curves for three Lubricants at (a) $F = 1800$ N and (b) $F = 4400$ N when $u_r = 30$ m/s and $\theta_{\text{lube}} = 40$ °C.

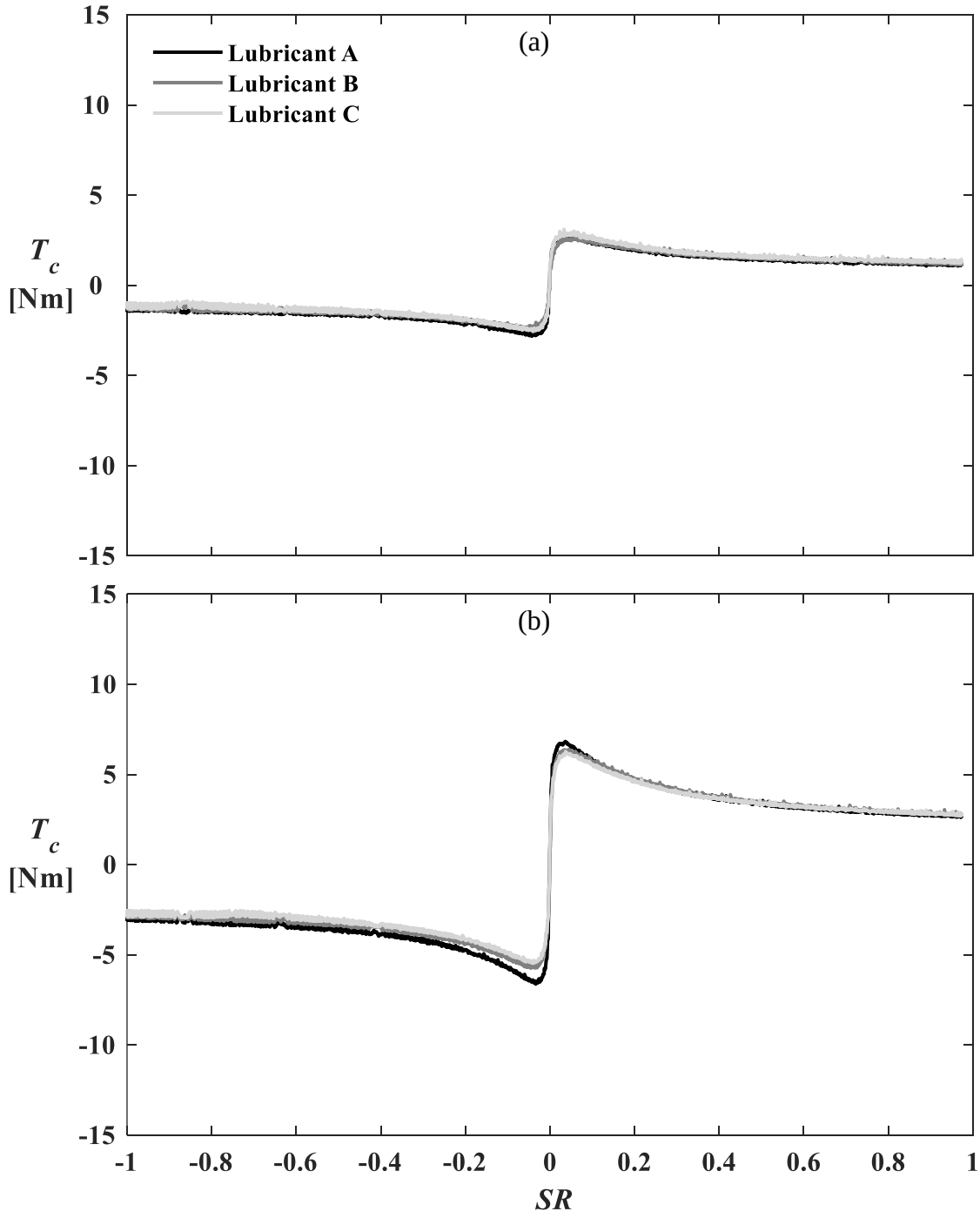

Figure 3.10: Comparison of measured T_c curves for three Lubricants at (a) $F = 1800$ N and (b) $F = 4400$ N when $u_r = 30$ m/s and $\theta_{\text{lube}} = 90$ °C.

Table 3.1: Summary of coefficient of friction μ from the traction tests of Figures 3.7 to 3.10.

				μ		
Lubricant	θ_{lube} [°C]	u_r [m/s]	$\sigma_{Hertzian}$ [GPa]	*SR*=0.05	*SR*=0.5	*SR*=1.0
A	40	10	1.9	0.050	0.024	0.018
			2.5	0.054	0.023	0.017
		30	1.9	0.039	0.014	0.011
			2.5	0.036	0.015	0.011
	90	10	1.9	0.042	0.025	0.018
			2.5	0.044	0.023	0.017
		30	1.9	0.028	0.015	0.012
			2.5	0.029	0.014	0.011
B	40	10	1.9	0.051	0.027	0.021
			2.5	0.055	0.025	0.018
		30	1.9	0.038	0.016	0.013
			2.5	0.037	0.015	0.012
	90	10	1.9	0.039	0.027	0.021
			2.5	0.040	0.024	0.018
		30	1.9	0.026	0.016	0.012
			2.5	0.027	0.015	0.012
C	40	10	1.9	0.045	0.025	0.019
			2.5	0.049	0.023	0.017
		30	1.9	0.034	0.015	0.013
			2.5	0.033	0.015	0.012
	90	10	1.9	0.030	0.022	0.018
			2.5	0.035	0.021	0.017
		30	1.9	0.029	0.016	0.013
			2.5	0.026	0.014	0.012

- Within the range $SR \subset [0.05, 0.5]$, Lubricants A and C had comparable friction performance with the an average coefficient of friction of $\bar{\mu} \approx 0.025$, followed by Lubricant B with $\bar{\mu} = 0.027$.

- Within the range $SR \subset [0.5, 1.0]$, the lowest average friction coefficient was $\bar{\mu} = 0.016$, $\bar{\mu} = 0.018$, and $\bar{\mu} = 0.018$ for Lubricants A, C, and B, respectively.

- An increase in θ_{lube} from 40 to 90 °C decreased μ by 21-27% at $SR = 0.05$ for the three lubricants, but had much less effect at $SR = 0.5$ and 1 (i.e. less than 4% decrease).

- Increasing F from 1800 to 4400 N increased μ by 2% at $SR = 0.05$, but decreased it by 4-10% at $SR = 0.5$ and 1 for each lubricant.

- Increasing u_r from 10 to 30 m/s had a significant impact on μ, decreasing μ by 22-40% at $SR = 0.05, 0.5$, and 1 for the three lubricants.

The summary of surface roughness values for the disk specimen pairs used in this study is shown in Table 3.2 and compares the arithmetic average surface roughness value R_a and root-mean-square surface roughness value R_q for axial and circumferential for pretest and posttest measurements. Based on Table 3.2, it is observed that pre and post-run disk pair specimens had comparable R_a and R_q values. This is the result of the disks being super-finished, where the peaks in surface finish remaining from machining have

Table 3.2: Summary of disk specimen roughness measurements and parameters.

		Ra [μm]				Rq [μm]			
		Axial		Circumferential		Axial		Circumferential	
Lubricant	Disk	Initial	Final	Initial	Final	Initial	Final	Initial	Final
A	C	0.036	0.039	0.049	0.049	0.046	0.048	0.063	0.060
	NC	0.027	0.025	0.034	0.032	0.035	0.032	0.043	0.041
B	C	0.038	0.036	0.044	0.040	0.049	0.045	0.057	0.051
	NC	0.030	0.021	0.037	0.034	0.039	0.027	0.048	0.044
C	C	0.033	0.034	0.034	0.029	0.042	0.047	0.044	0.038
	NC	0.025	0.024	0.033	0.031	0.033	0.030	0.041	0.039

already been removed, negating the necessity to run-in the surfaces. Initial and final macroscopic and microscopic digital images for the disk pairs used for each lubricant are displayed in Figure 3.11 to 3.13.

3.3 Multiple Linear Regression of Measured Traction Curves

Multiple linear regression is used to model predict values of a response variable (dependent) from predicter variables (independent) x_i, their regression coefficients β_i, and an error term ε. The "true" regression line equation is

$$y_i = \beta_0 + \beta_1 x_{i1} + \beta_2 x_i + ... + \beta_p x_{ip} + \varepsilon_i, \tag{3.2}$$

where y_i is the response variable T_c or a function of T_c when a transformation is applied, and β_0 is the y-intercept. Due to measurement error, the regression coefficients β_i must be estimated with $\hat{\beta}_i$ in a least squares line equation defined as

$$\hat{y}_i = \hat{\beta}_0 + \hat{\beta}_1 x_{i1} + \hat{\beta}_2 x_{i2} + ... + \hat{\beta}_p x_{ip}. \tag{3.3}$$

The coefficient of determination R^2 is used to access the goodness of fit of a regression model and is the ratio of variance in the response variable that is from the predictor variables. R^2 is limited in that is sensitive to outliers and inherently increases when an additional predictor variable is introduced in the model. Thus, an adjusted R^2 (R^2_{adj}) value is used, which does not increase unless the added predictor variable has contribution to the model.

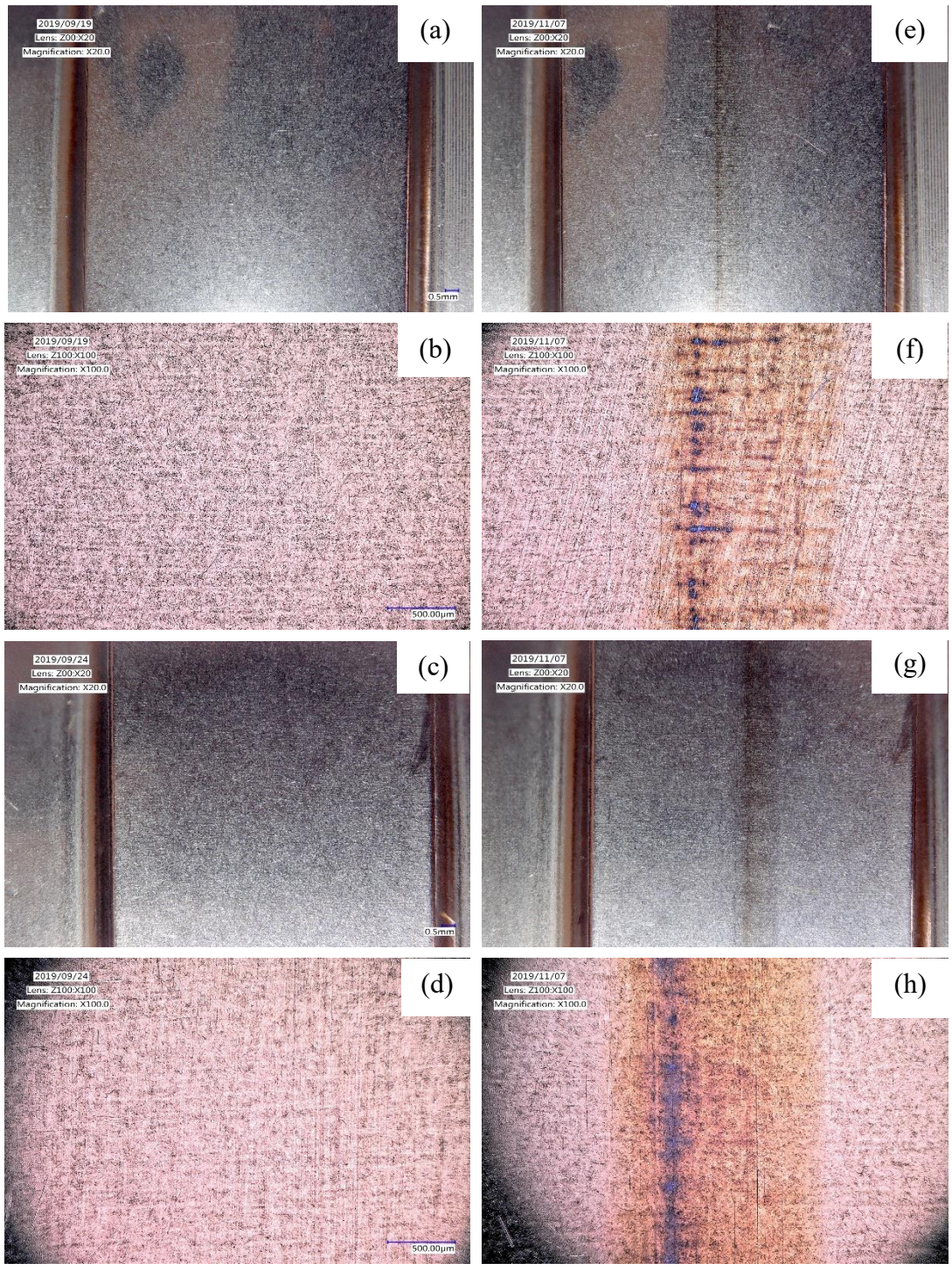

Figure 3.11: Initial (a-d) and final (e-h) macroscopic (a,c,e,g) and microscopic (b,d,f,h) digital images of the crowned (a-b,e-f) and non-crowned (c-d,g-h) disk surfaces for Lubricant A.

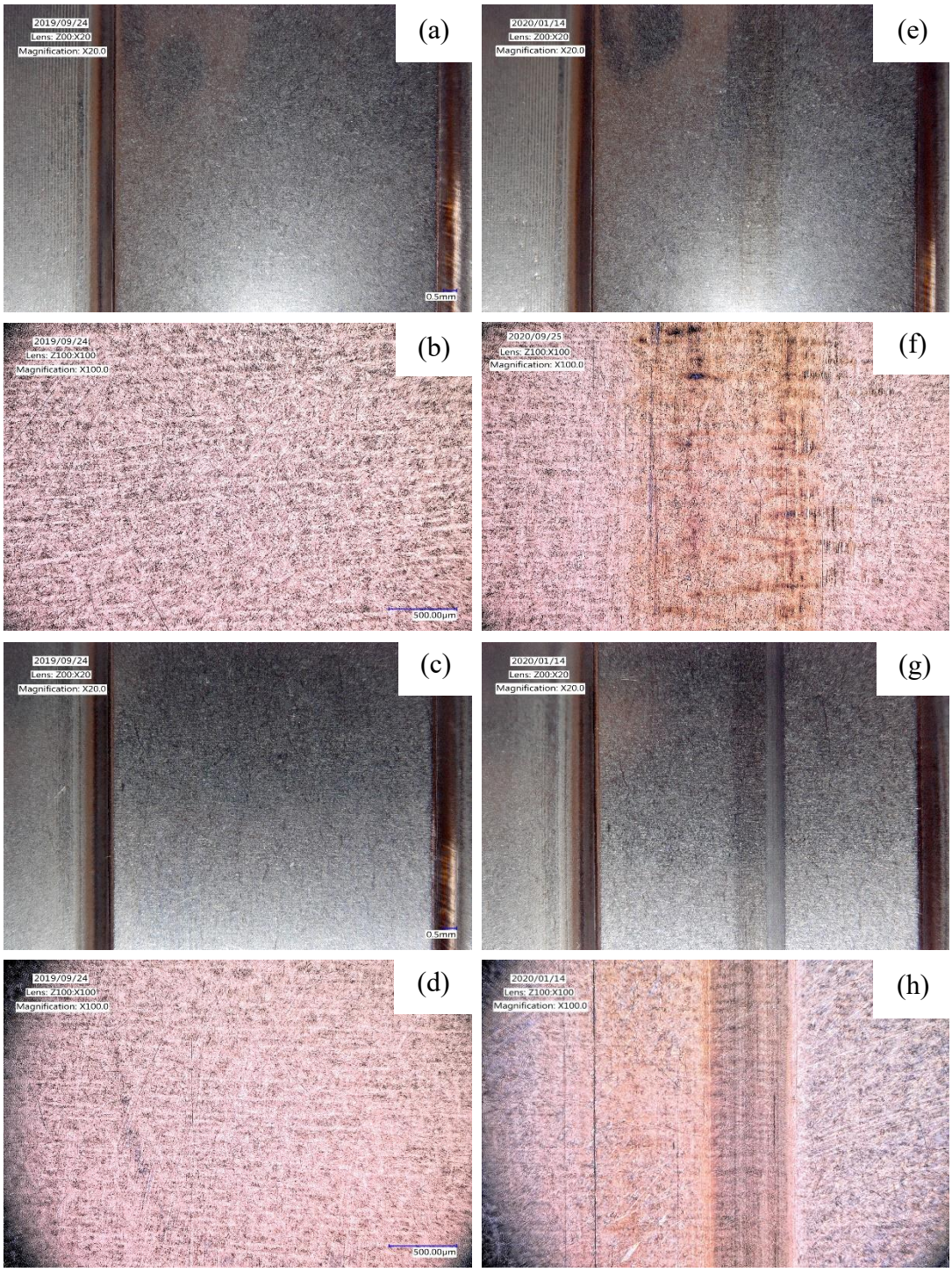

Figure 3.12: Initial (a-d) and final (e-h) macroscopic (a,c,e,g) and microscopic (b,d,f,h) digital images of the crowned (a-b,e-f) and non-crowned (c-d,g-h) disk surfaces for Lubricant B.

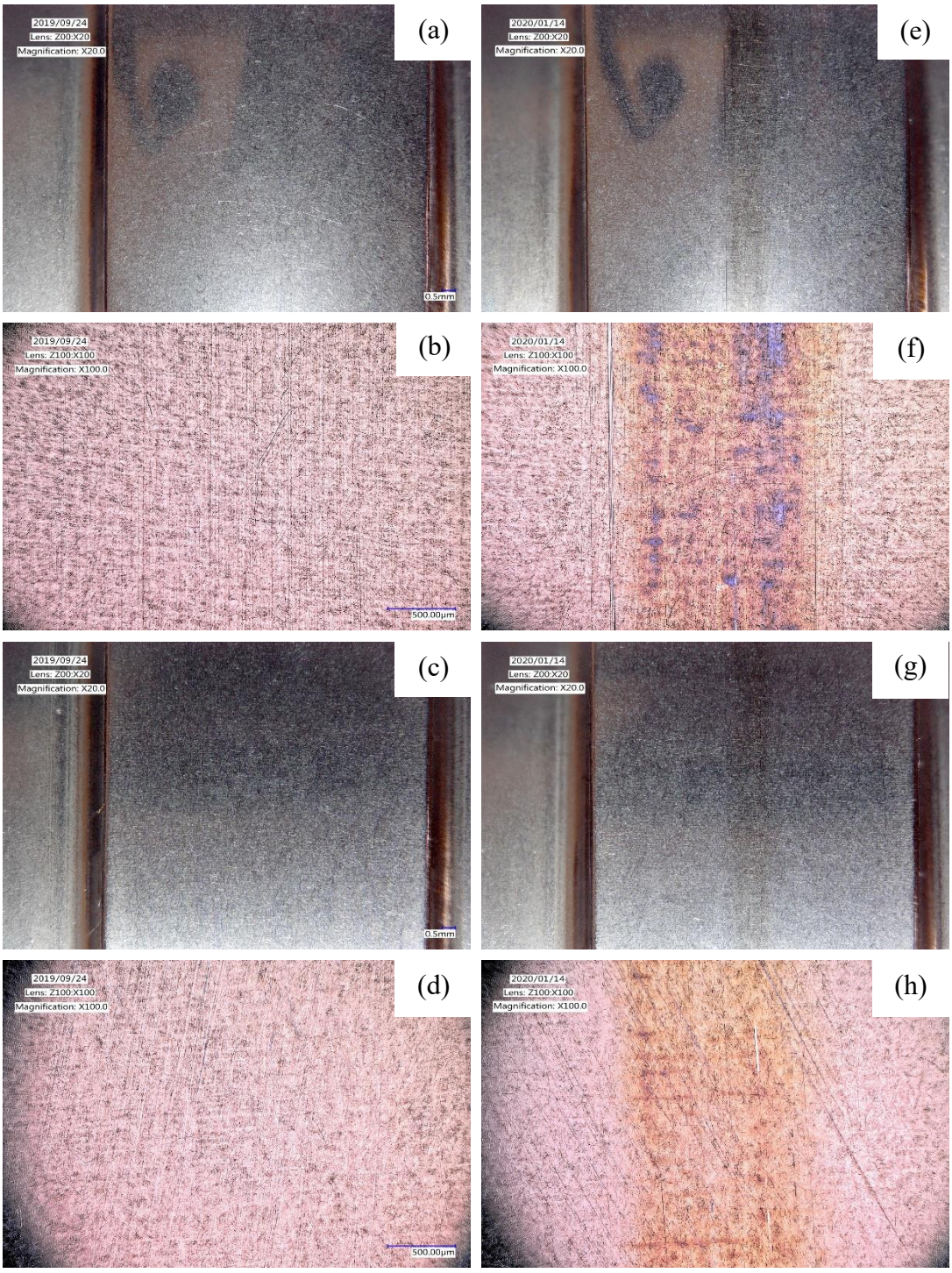

Figure 3.13: Initial (a-d) and final (e-h) macroscopic (a,c,e,g) and microscopic (b,d,f,h) digital images of the crowned (a-b,e-f) and non-crowned (c-d,g-h) disk surfaces for Lubricant C.

The original predictor (independent) variables are F, u_r, SR, and θ_{lube} while the response (dependent) variable is T_c or μ. In order to accurately account for disk specimen material and geometry, normal force F is replaced with its corresponding σ_{Hertzian}. θ_{lube} is replaced by its corresponding ambient lubricant low shear viscosity η_i shown in Table 3.3.

Minitab was used to perform a multiple linear regression of the traction data to describe the relationships between predicator and response variables described in Section 3.2. The measurements used within the regression analyses are displayed in Table 3.1. A regression was first performed including all three oils, but the overall shape of the fitted curves did not accurately match the measured traction curves. This was likely a result of the role lubricant specific additives has in each oil that were not quantified and included in the regression. Thus, a regression was performed for each individual oil. For Lubricant A, the regression equation is selected as

$$\begin{aligned}\ln(T_c) = {} & \hat{\beta}_0 + \hat{\beta}_1 SRu_r + \hat{\beta}_2 SR\eta + \hat{\beta}_3 \sigma_{\text{Hertzian}} \ln(\sigma_{\text{Hertzian}}) - \\ & \hat{\beta}_4 \sigma_{\text{Hertzian}} \ln(SR) + \hat{\beta}_5 u_r \ln(SR) - \hat{\beta}_6 \ln(SR)^2 - \\ & \hat{\beta}_7 \ln(u_r)^2 - \hat{\beta}_8 \ln(SR)\ln(u_r) - \hat{\beta}_9 \ln(SR)\ln(\eta).\end{aligned} \tag{3.4}$$

The corresponding regression equation estimated coefficients $\hat{\beta}_i$ are shown in Table 3.5. Similarly, the regression equations for Lubricant B and Lubricant C are selected as

$$\begin{aligned}\ln(T_c) = {} & \hat{\beta}_0 + \hat{\beta}_1 \sigma_{\text{Hertzian}} \eta + \hat{\beta}_2 SRu_r - \hat{\beta}_3 SR\eta + \hat{\beta}_4 \sigma_{\text{Hertzian}}{}^2 - \\ & \hat{\beta}_5 \sigma_{\text{Hertzian}} \ln(SR) - \hat{\beta}_6 SR\ln(u_r) - \hat{\beta}_7 u_r \ln(SR) - \hat{\beta}_8 u_r \ln(u_r)\end{aligned} \tag{3.5}$$

and

Table 3.3: Lubricant properties at respective temperatures for the three lubricants used in this study.

Property	Units	Symbol	θ_{lube} [°C]	Lubricant A	Lubricant B	Lubricant C
Ambient Low Shear Viscosity	Pa·s	η_i	40	0.146	0.078	0.108
			70	0.032	0.020	0.027
			90	0.015	0.010	0.014
Relative Density	kg/m^3	ρ_i	40	835.4	825.6	826.1
			70	817.9	807.6	807.9
			90	806.3	795.6	795.8

Table 3.4: Matrix of parameters used for multiple linear regression.

Lubricants	A, B, C
θ_{lube} [°C]	40, 90
$\sigma_{Hertzian}$ [GPa]	1.9, 2.5
u_r [m/s]	10, 30
SR	0.06, 0.015 0.3, 0.5, 0.7, 0.95

Table 3.5: Regression coefficients for the Lubricants used in the study.

	Lubricant		
Estimated Coefficient	A	B	C
$\hat{\beta}_0$	0.1559	0.2415	0.2874
$\hat{\beta}_1$	0.0157	1.1715	-0.0065
$\hat{\beta}_2$	0.2575	0.0242	-0.0168
$\hat{\beta}_3$	0.7132	-3.0608	0.0805
$\hat{\beta}_4$	-0.0399	0.2592	1.1213
$\hat{\beta}_5$	0.0127	-0.0566	1.7665
$\hat{\beta}_6$	-0.0874	-0.2333	-0.1508
$\hat{\beta}_7$	0.1156	-0.0046	-0.0007
$\hat{\beta}_8$	-0.3158	-0.0086	0.0130
$\hat{\beta}_9$	-0.0182	--	-0.0023

$$\ln(T_c) = \hat{\beta}_0 - \hat{\beta}_1 u_r - \hat{\beta}_2 SR u_r + \hat{\beta}_3 SR\eta - \hat{\beta}_4 \eta \ln(SR) + \hat{\beta}_5 \ln(\sigma_{\text{Hertzian}})^2 - \hat{\beta}_6 \ln(\sigma_{\text{Hertzian}}) \ln(SR) - \hat{\beta}_7 \sigma_{\text{Hertzian}}{}^2 u_r + \hat{\beta}_8 SR u_r - \hat{\beta}_9 u_r{}^2 \eta. \quad (3.7)$$

These regressions resulted in R^2_{adj} values of 0.999, 0.996, and 0.995, respectively, for the traction curves outlined in Table 3.1. A comparison of measured contact torque T_c and fitted contact torque $\hat{T}_c$ for $SR > 0$ is shown in Figures 3.14 to Figure 3.22 for all the traction tests performed. The fitted values mostly coincide with the measured data, suggesting a good fit. The traction curves that do not agree well are when the applied normal load was $F = 500$ N $(\sigma_{\text{Hertzian}} = 1.2$ GPa). This is probably attributable to less heat generation, causing less shear thinning, which results in these traction curves having a qualitatively different shape. These differences are amplified because none of the $F = 500$ N experimental data was used in the regression as displayed in Table 3.1. The lower heat generation is apparent in Figure 3.23 - Figure 3.28(a-b), which compare measured contact torque and their associated surface bulk temperature between the disk specimens at selected test conditions for each lubricant.

3.4 Summary

This chapter presented families of measured traction curves at conditions defined in Table 2.2 along with associated trends in T_c based on F, u_r, SR, and θ_{lube}. Measurement repeatability was validated and comparisons in measured coefficient friction between lubricants were made. Linear regression methodology and closed form formulae

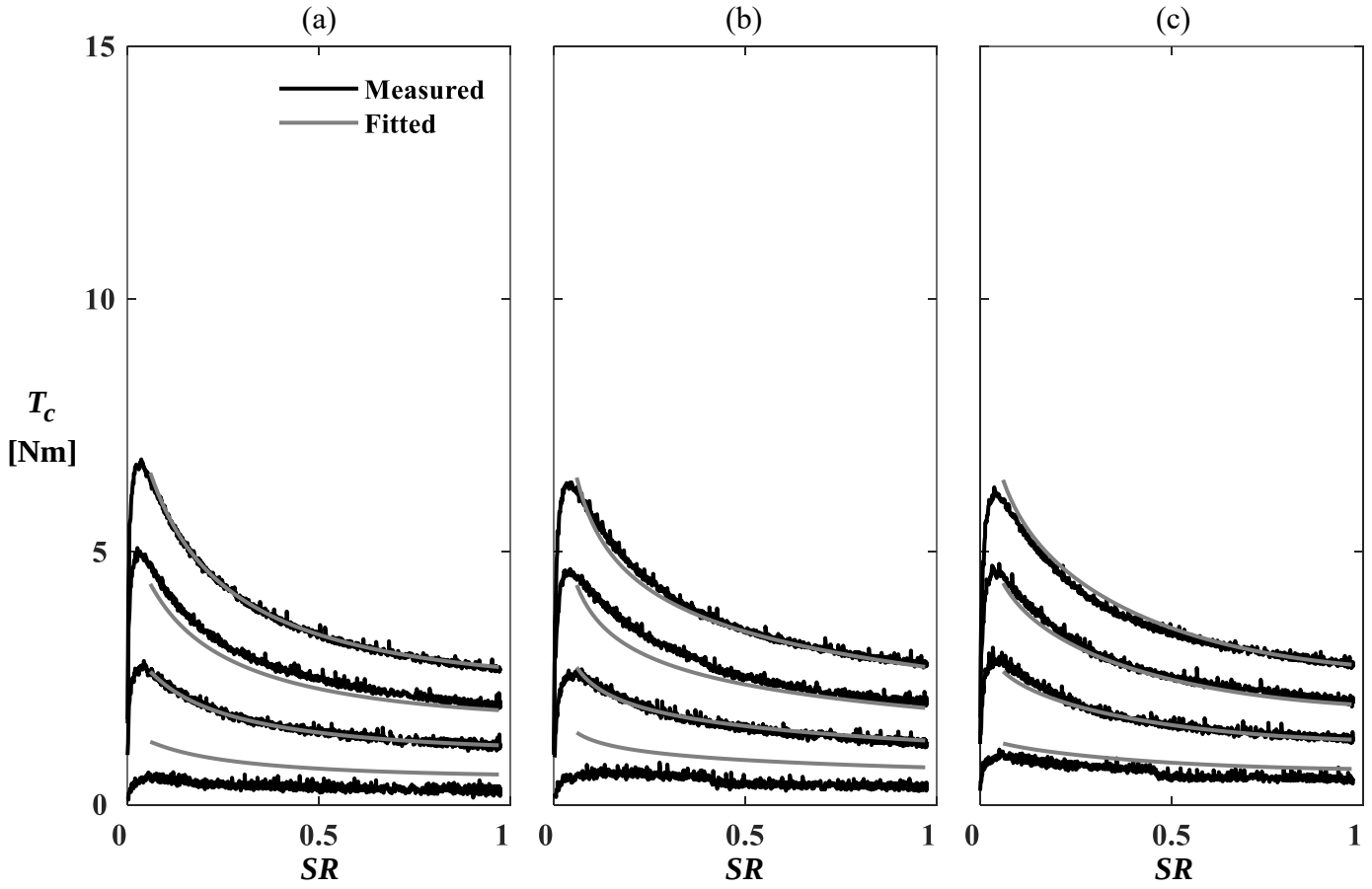

Figure 3.14: Comparison of measured and fitted contact torque for (a) Lubricant A, (b) Lubricant B, and (c) Lubricant C at $u_r = 30$ m/s and $\theta_{\text{lube}} = 90$ °C.

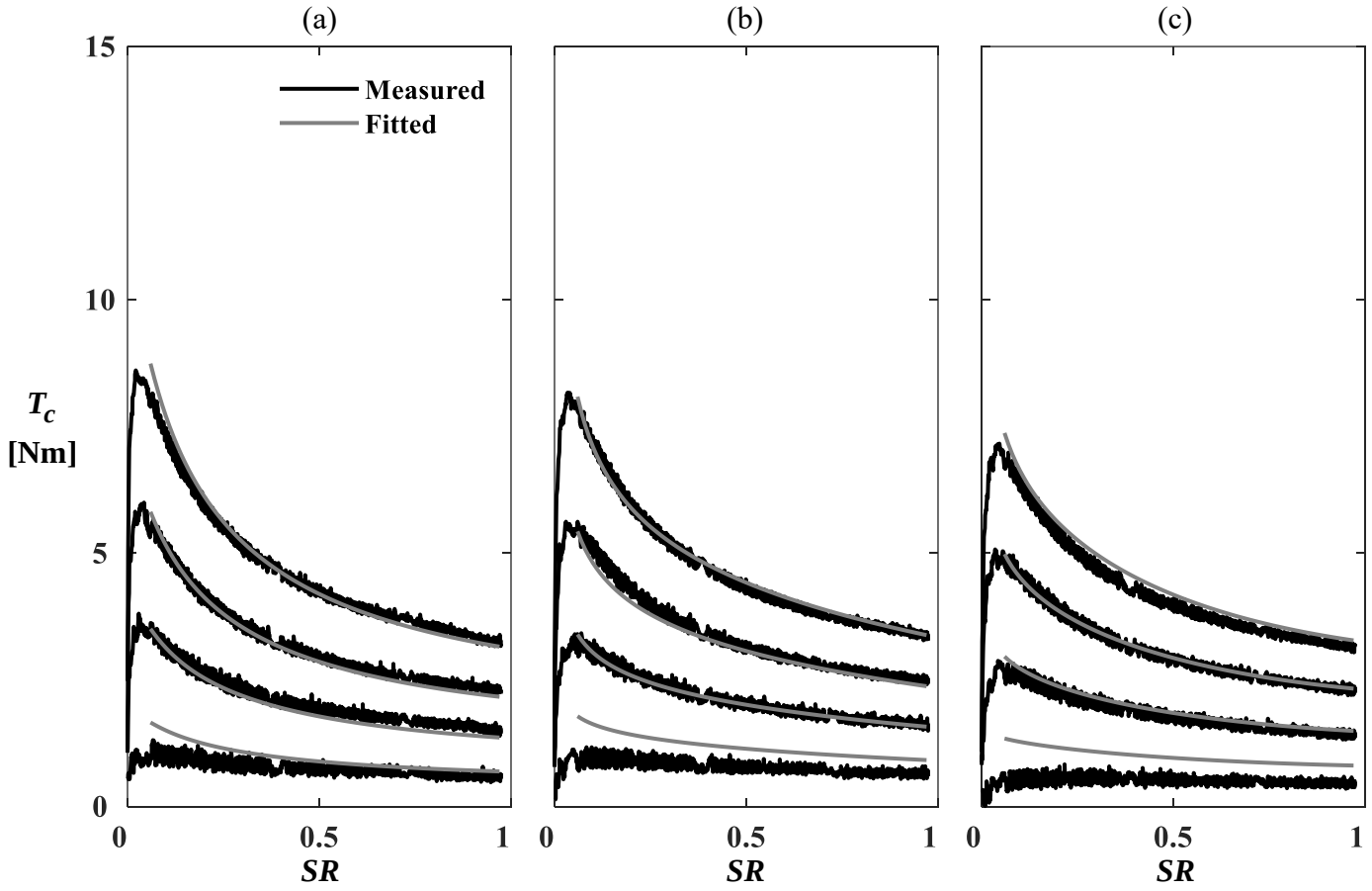

Figure 3.15: Comparison of measured and fitted contact torque for (a) Lubricant A, (b) Lubricant B, and (c) Lubricant C at $u_r = 20$ m/s and $\theta_{\text{lube}} = 90$ °C.

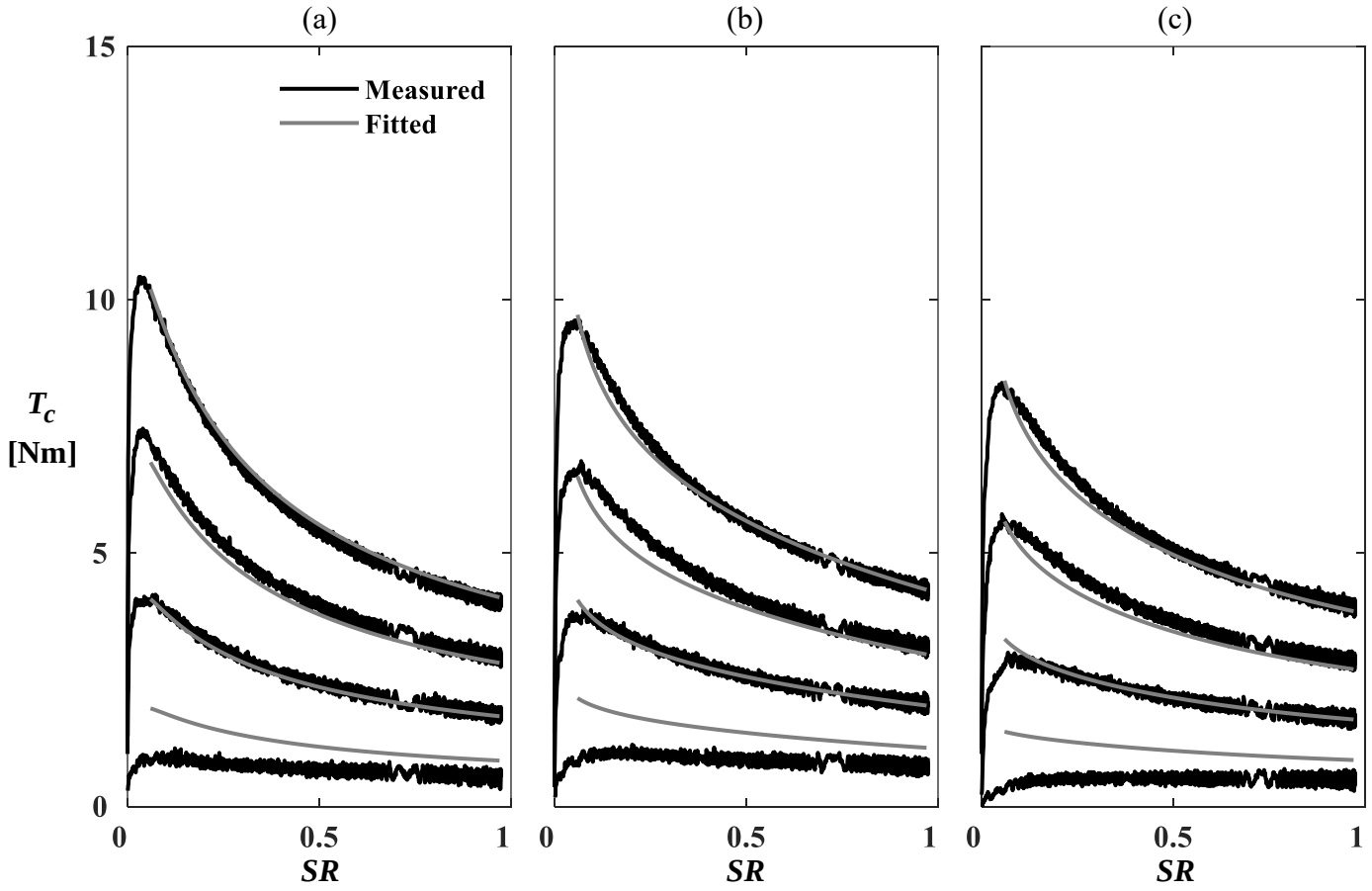

Figure 3.16: Comparison of measured and fitted contact torque for (a) Lubricant A, (b) Lubricant B, and (c) Lubricant C at $u_r = 10$ m/s and $\theta_{\text{lube}} = 90$ °C.

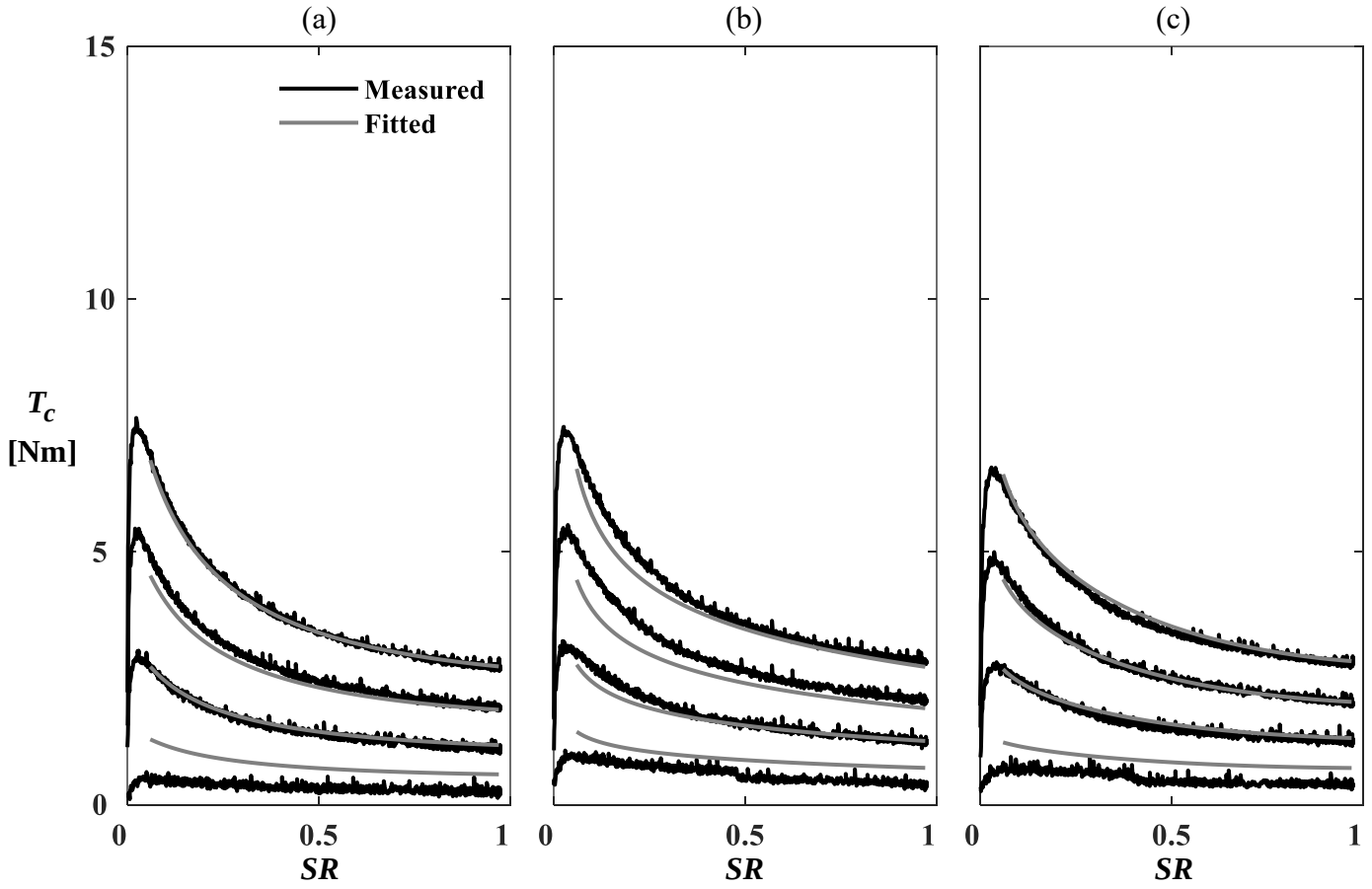

Figure 3.17: Comparison of measured and fitted contact torque for (a) Lubricant A, (b) Lubricant B, and (c) Lubricant C at $u_r = 30$ m/s and $\theta_{\text{lube}} = 70$ °C.

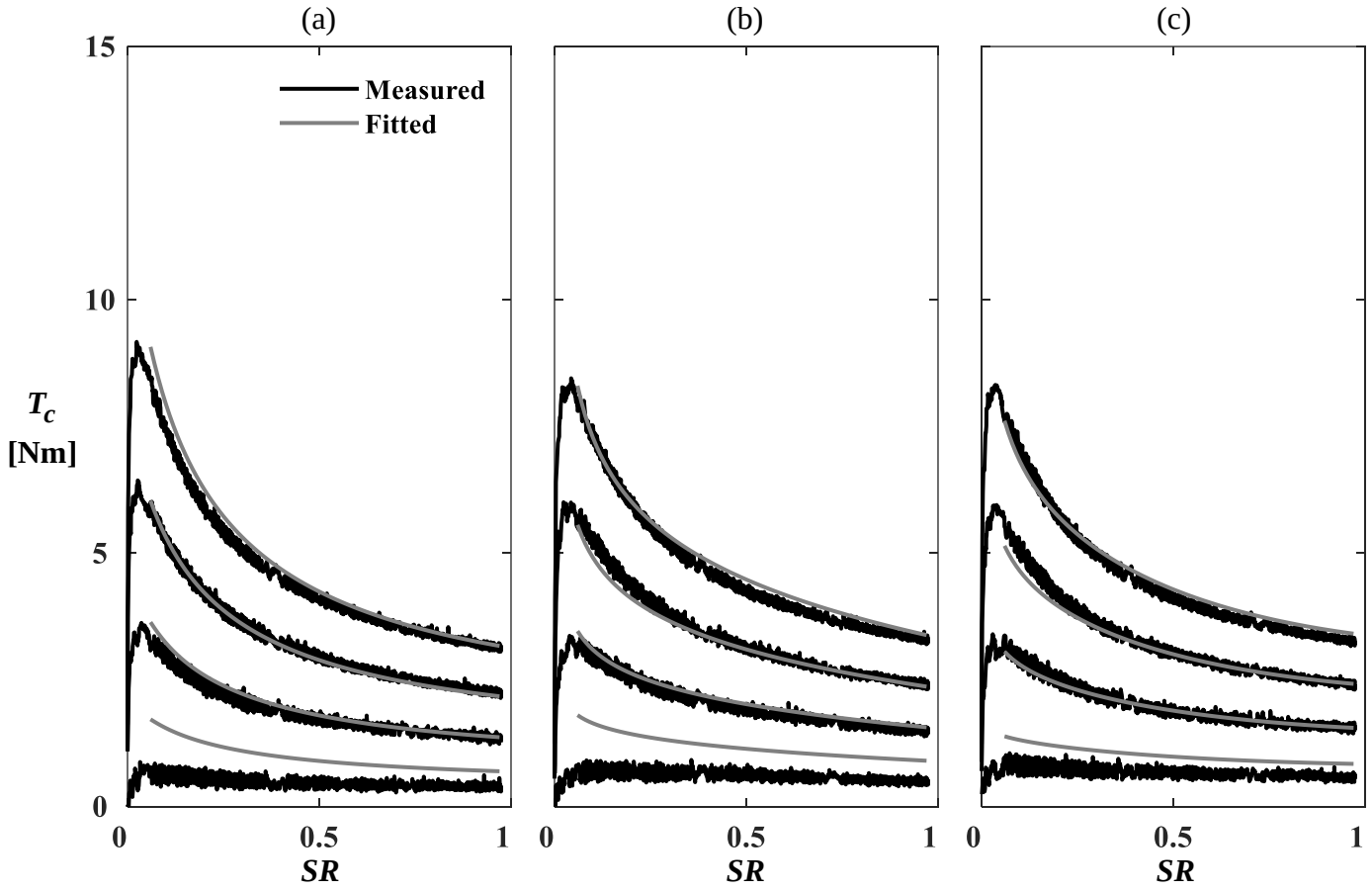

Figure 3.18: Comparison of measured and fitted contact torque for (a) Lubricant A, (b) Lubricant B, and (c) Lubricant C at $u_r = 20$ m/s and $\theta_{\text{lube}} = 70$ °C.

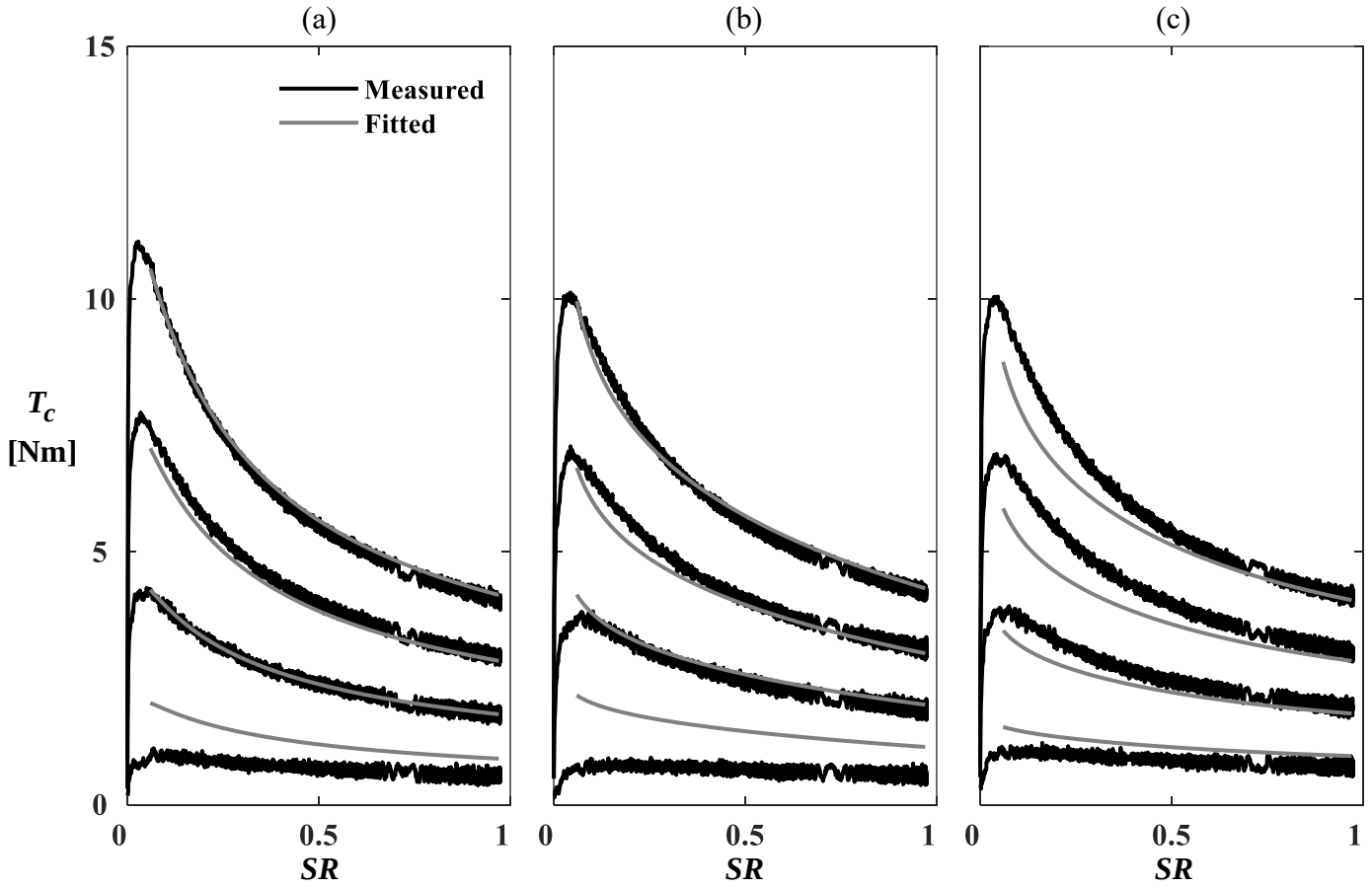

Figure 3.19: Comparison of measured and fitted contact torque for (a) Lubricant A, (b) Lubricant B, and (c) Lubricant C at $u_r = 10$ m/s and $\theta_{\text{lube}} = 70$ °C.

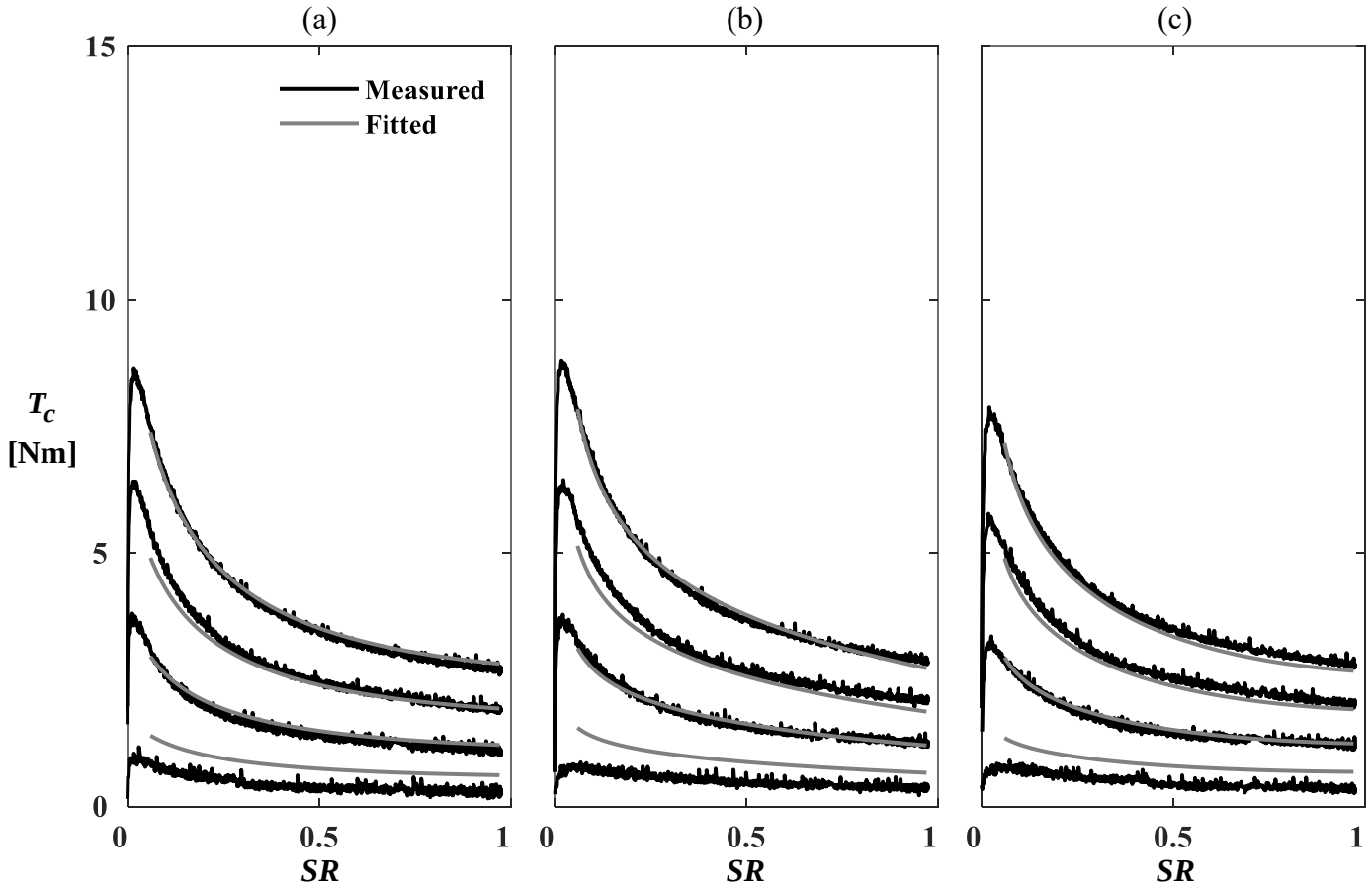

Figure 3.20: Comparison of measured and fitted contact torque for (a) Lubricant A, (b) Lubricant B, and (c) Lubricant C at $u_r = 30$ m/s and $\theta_{\text{lube}} = 40$ °C.

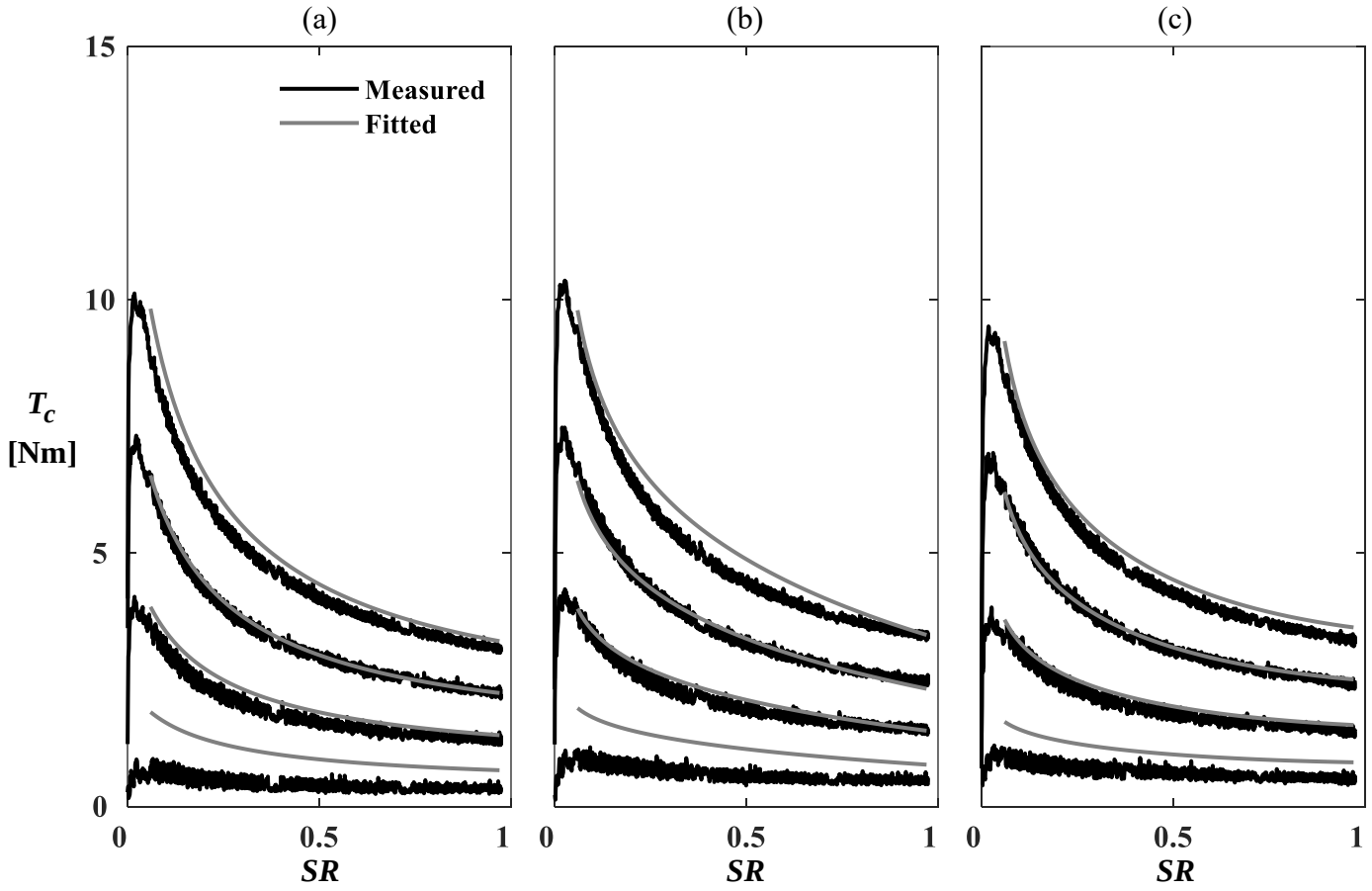

Figure 3.21: Comparison of measured and fitted contact torque for (a) Lubricant A, (b) Lubricant B, and (c) Lubricant C at $u_r = 20$ m/s and $\theta_{\text{lube}} = 40$ °C.

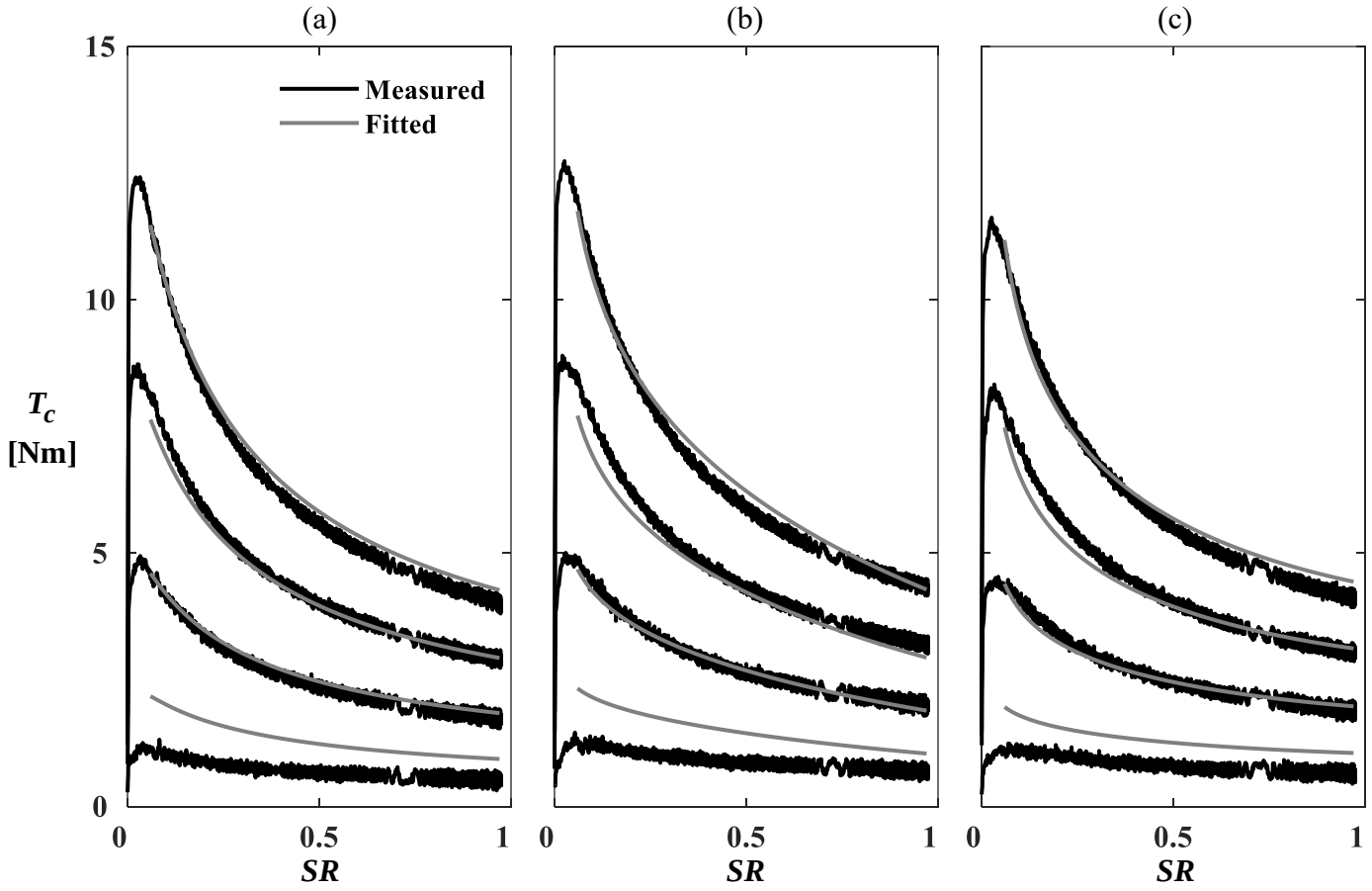

Figure 3.22: Comparison of measured and fitted contact torque for (a) Lubricant A, (b) Lubricant B, and (c) Lubricant C at $u_r = 10$ m/s and $\theta_{\text{lube}} = 40$ °C.

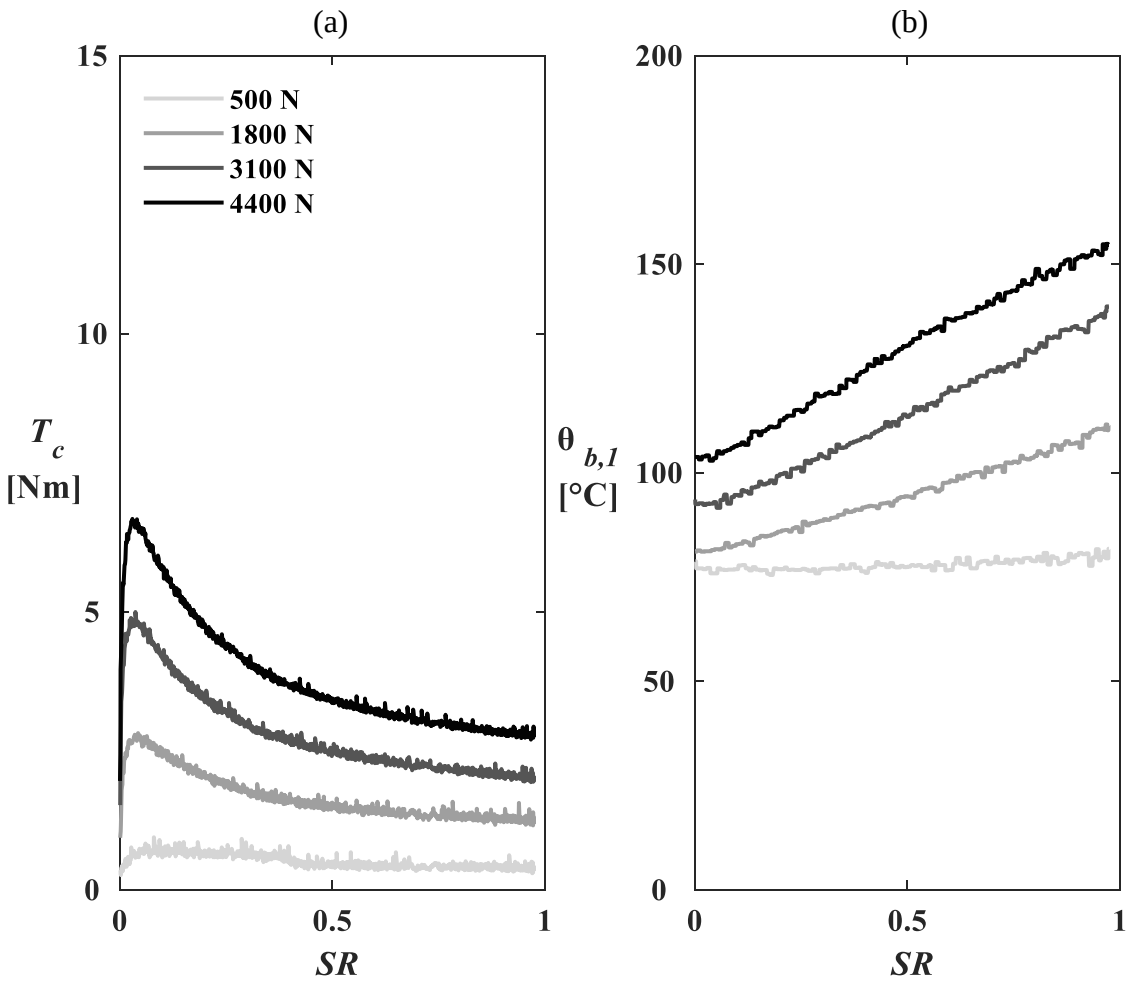

Figure 3.23: Comparison of (a) measured contact torque T_c and (b) corresponding surface bulk temperatures $\theta_{b,1}$ for Lubricant C at $u_r = 30$ m/s and $\theta_{\text{lube}} = 70$ °C.

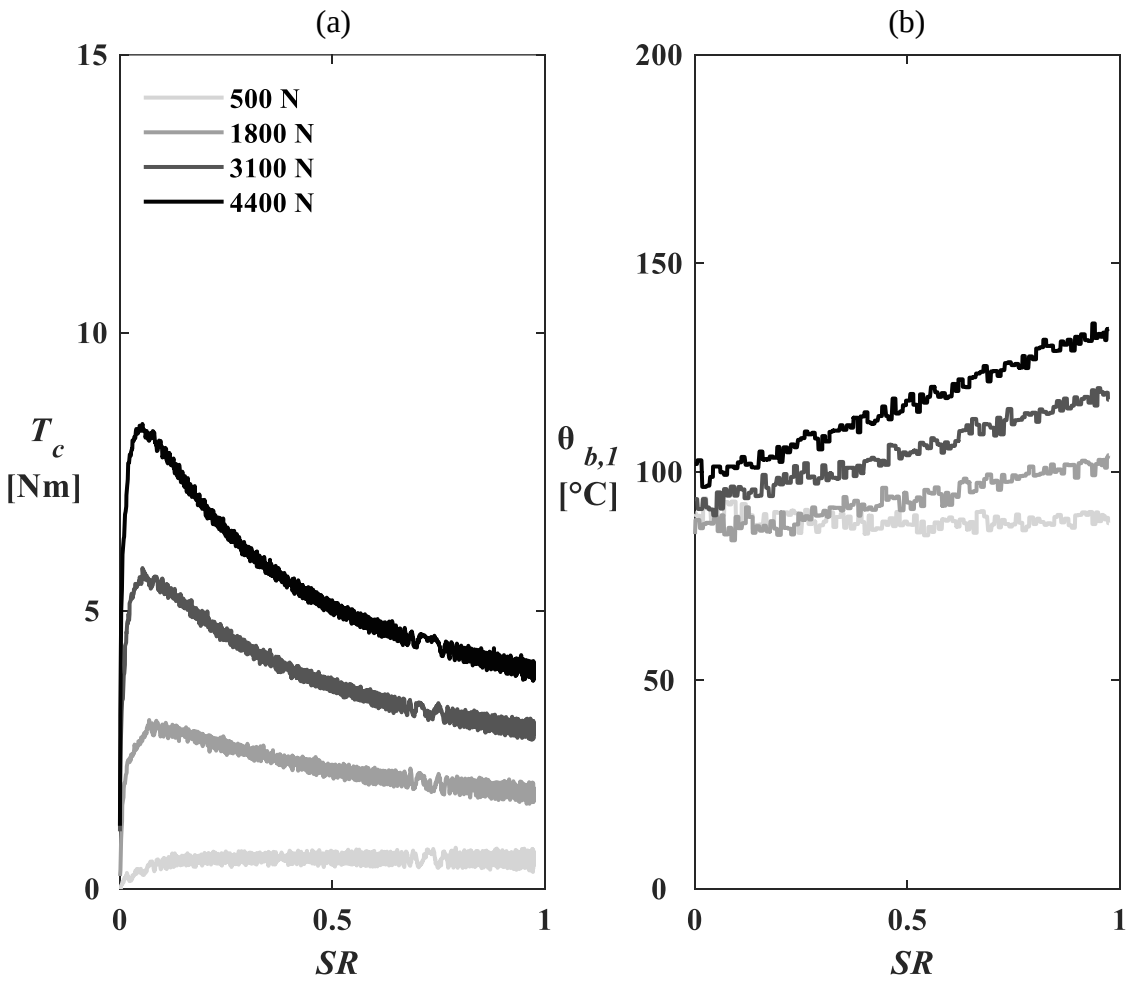

Figure 3.24: Comparison of (a) measured contact torque T_c and (b) corresponding surface bulk temperatures $\theta_{b,1}$ for Lubricant C at $u_r = 10$ m/s and $\theta_{\text{lube}} = 90$ °C.

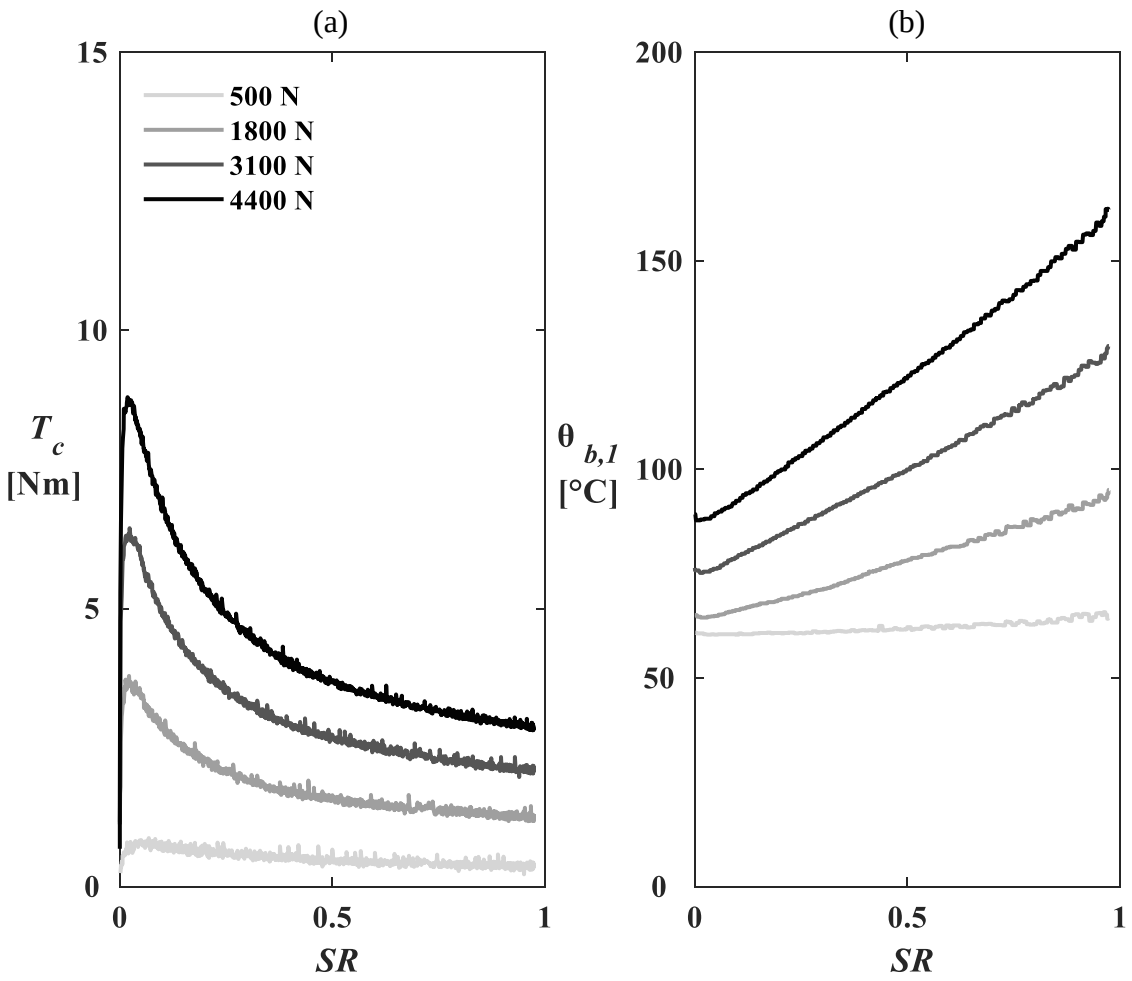

Figure 3.25: Comparison of (a) measured contact torque T_c and (b) corresponding surface bulk temperatures $\theta_{b,1}$ for Lubricant B at $u_r = 30$ m/s and $\theta_{\text{lube}} = 40$ °C.

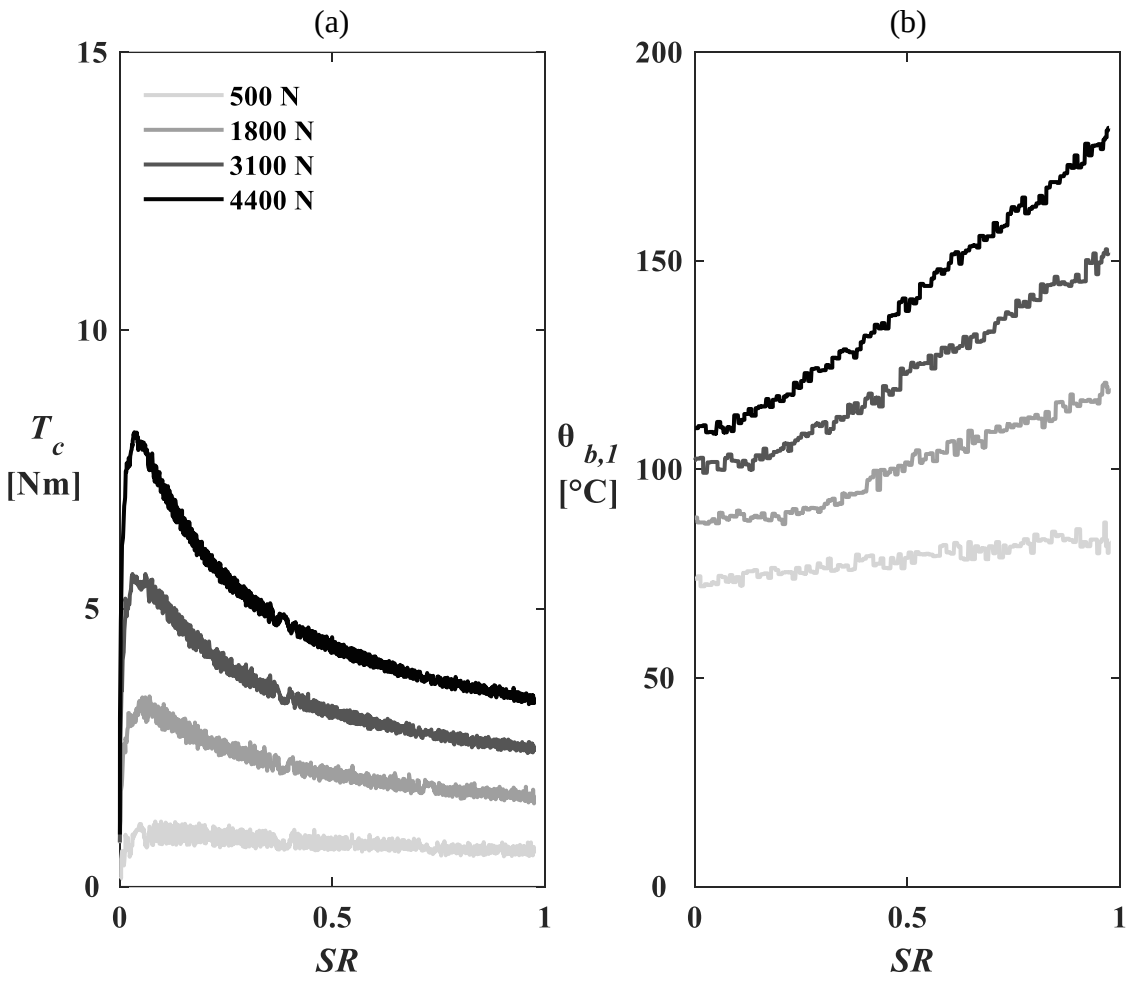

Figure 3.26: Comparison of (a) measured contact torque T_c and (b) corresponding surface bulk temperatures $\theta_{b,1}$ for Lubricant B at $u_r = 20$ m/s and $\theta_{\text{lube}} = 90$ °C.

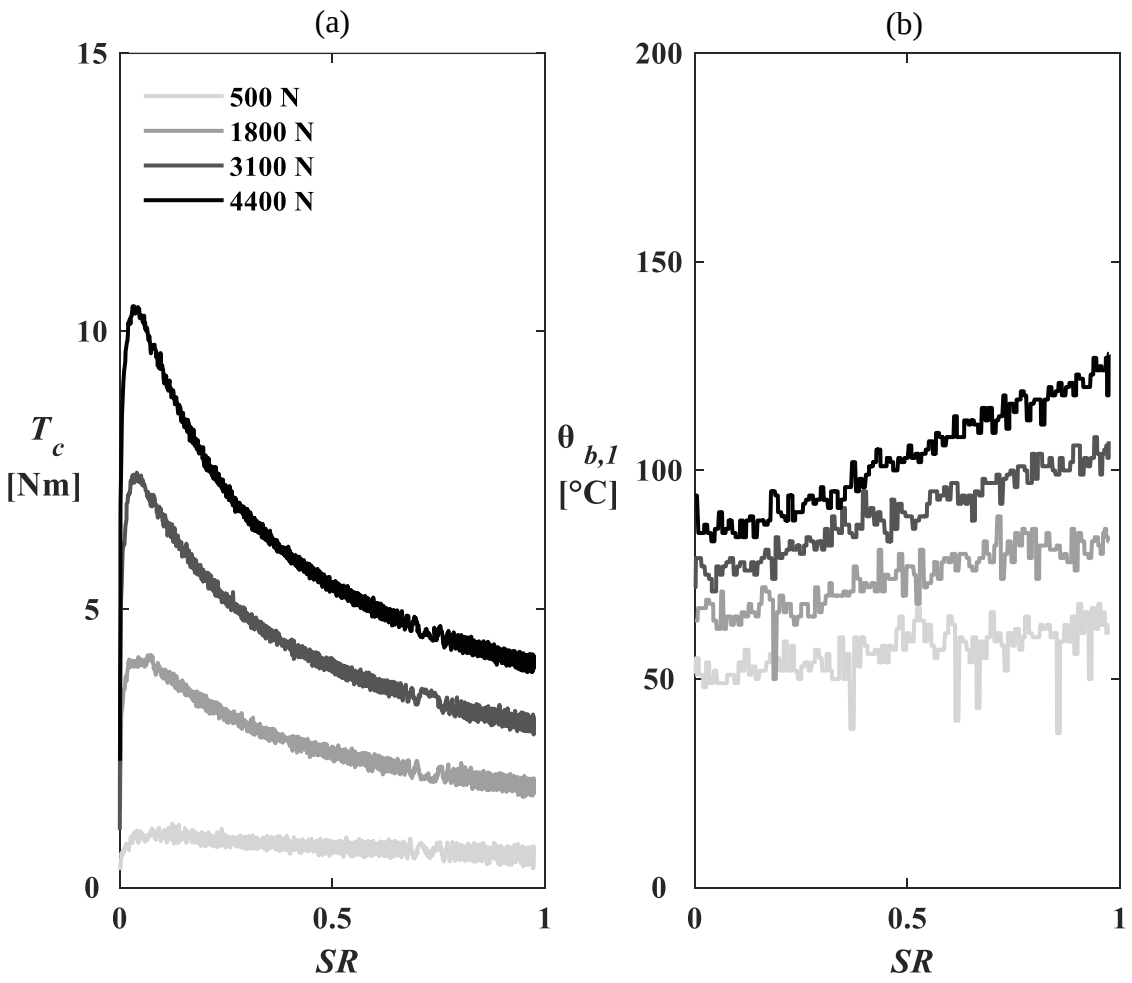

Figure 3.27: Comparison of (a) measured contact torque T_c and (b) corresponding surface bulk temperatures $\theta_{b,1}$ for Lubricant A at $u_r = 10$ m/s and $\theta_{\text{lube}} = 90$ °C.

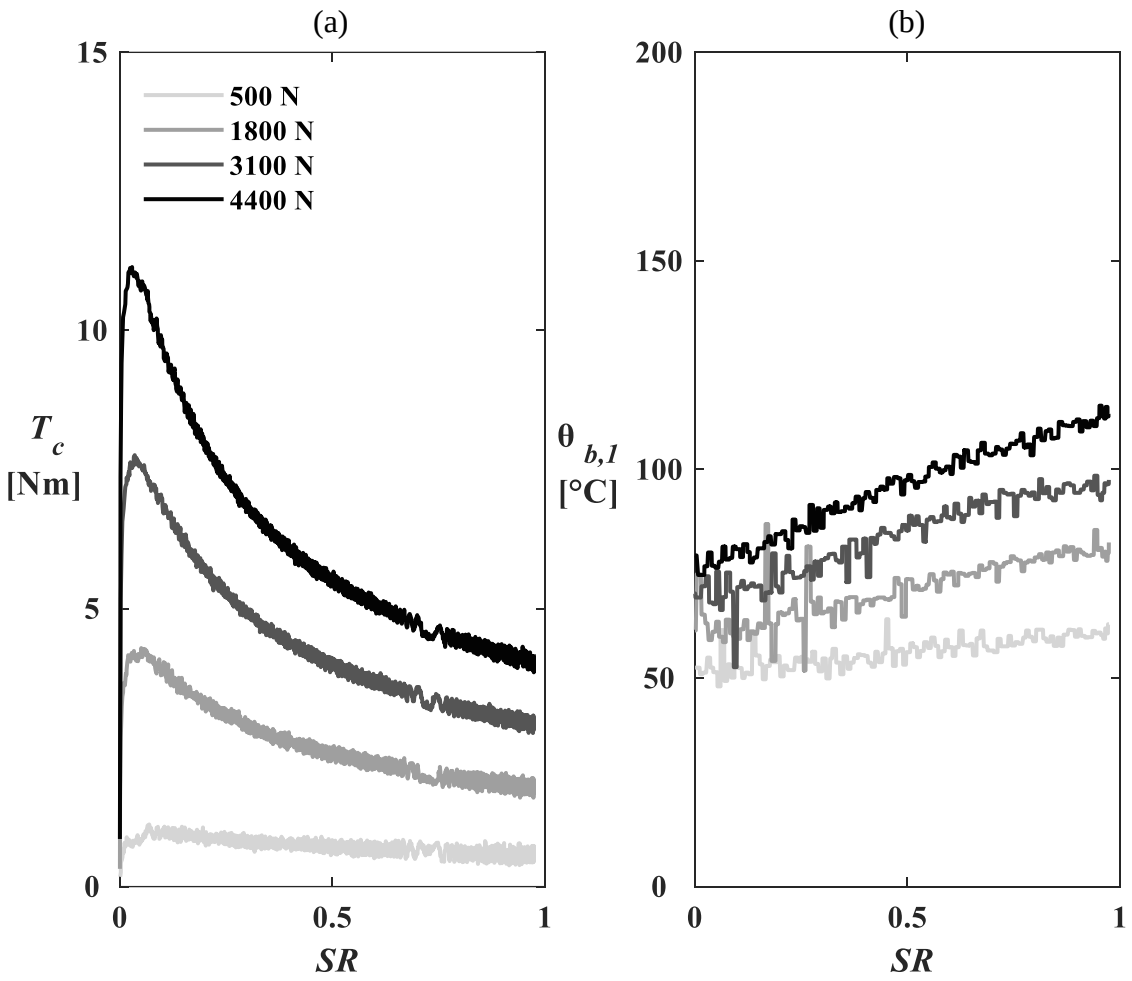

Figure 3.28: Comparison of (a) measured contact torque T_c and (b) corresponding surface bulk temperatures $\theta_{b,1}$ for Lubricant A at $u_r = 10$ m/s and $\theta_{\text{lube}} = 70$ °C.

for T_c were described and chosen. Overall, it was observed that all three lubricants represent similar traction behavior.

CHAPTER 4

CONCLUSION

4.1 Summary

This experimental study consisted of evaluating the friction performance of three automotive transmission fluids with super-finished automotive grade gear steel disk specimens. Various combinations of operating conditions were tested to cover a wide range of automotive operating conditions using a twin-disk, high-speed tribometer setup. 36 unique traction tests were conducted for each lubricant. All disk specimens were inspected for their roughnesses by using a surface contact profilometer and a non-contact optical profiler. In addition, digital microscopic and macroscopic images of the contact surfaces were captured before and after all traction tests were performed. It was hypothesized that disk specimen surface roughness was not expected to change throughout the duration of the traction tests due to their chemically polished surfaces and was confirmed with the inspection procedure. The results were presented for direct comparison between lubricants at equivalent operating conditions.

Generating a database of lubricant experimental data was essential to develop regressed friction equations. These equations are to be used for estimation for (i) simplistic model input or (ii) validation for complex EHL models. The effects of the independent test parameters, namely F $(\sigma_{\text{Hertzian}})$, θ_{lube} (η), u_r, and SR were quantified and modeled to predict contact torque for each lubricant. Additives were not quantified, so separate regression analyses were completed to improve the qualitative shape and fit of the curves.

4.2 Major Conclusions

From the results displayed in Chapter 3, the major conclusions regarding the traction tests performed with the high-speed, twin-disk tribometer are as follows:

- The test methodology adapted from Handschuh et al. [7] and bearing loss removal procedure was found to be satisfactory and repeatable in assessing traction performance for automotive transmission fluids operating at a wide variety of conditions.
- All three lubricants had similar traction performance across most of the test conditions in this study except for low values of SR, in which Lubricant C had superior performance compared to the other two lubricants.
- Increasing u_r had the most significant impact on μ inside the range of $SR \subset [0.05, 1.0]$, decreasing μ by 22-40%, while the effects of θ_{lube} and F $(\sigma_{\text{Hertzian}})$ were low to moderate for each lubricant.

- The regressed closed-form formulae for measured contact torque T_c agree well with the experimental data with minor deviations evident in low load cases $F = 500$ N $(\sigma_{\text{Hertzian}} = 1.2$ GPa$)$. Consequently, simplified efficiency calculations can be executed, and direct comparisons EHL models can be made.

4.3 Recommendations for Future Work

The following list describes several ways the research in this study can be further developed and expanded upon:

- A study incorporating the effects of disk specimen surface roughness might better differentiate the traction performance of the lubricants used in this study.
- This study was only concerned with the frictional performance of the lubricant. Conducting surface fatigue and scuffing performance experiments would be necessary to fully evaluate each lubricant's overall performance.
- The experimental traction results and empirical regression data can be used to validate and update existing EHL models for high speed automotive operating conditions.
- This study used the ambient low shear viscosity to characterize each lubricant at the respective test conditions for the regression analysis, which may not be the most accurate way to represent the fluids. Including the pressure-temperature effects of viscosity or including lubricant additives could be more representative of the lubricant, leading to more accurate empirical regression formulae.

REFERENCES

[1] Riggs, M. R., Murthy, N. K., and Berkebile, S. P., “Scuffing Resistance and Starved Lubrication Behavior in Helicopter Gear Contacts: Dependence on Material, Surface Finish, and Novel Lubricants,” *Tribology Transactions*, **60**(5), p. 932–941, 2017.

[2] Li, S., Kahraman, A., Anderson, N., and Wedeven, L. D., “A Model to Predict Scuffing Failures of a Ball-On-Disk Contact,” *Tribology International*, **60**, p. 233–245, 2013.

[3] Wedeven, L. D., "Traction and Film Thickness Measurements Under Starved Elastohydrodynamic Conditions," *Journal of Lubrication Technology*, **97** (2), 321-329, 1975.

[4] Wedeven, L. D., Black, W. F., and Carlisle, D. J., “Tribology Testing of Advanced Aviation Oils, Bearing and Gear Materials,” Proceedings of the World Tribology Congress III - 2005, p. 673–674, 2005.

[5] Werner, P., Altstädt, V., Jaskulka, R., Jacobs, O., Sandler, J. K. W., Shaffer, M. S. P., and Windle, A. H., “Tribological Behaviour of Carbon-Nanofibre-Reinforced Poly(Ether Ether Ketone),” *Wear*, **257**(9–10), p. 1006–1014, 2004.

[6] Liou, J. J., “A Theoretical and Experimental Investigation of Roller and Gear Scuffing,” Ph.D. Dissertation, The Ohio State University, Columbus, Ohio, 2010.

[7] Handschuh, M. J., Kahraman, A., and Anderson, N. E., “Development of a High-Speed Two-Disc Tribometer for Evaluation of Traction and Scuffing of Lubricated

Contacts," *Tribology Transactions*, **63**(3), p. 509–518, 2020.

[8] Wilson, S., "Traction and Wear Evaluation of a Number of Plastic Materials and Greases under Combined Rolling and Sliding Contact Conditions," M.S Thesis, The Ohio State Unviersity, Columbus, Ohio, 2012.

[9] Patching, M. J., Kewh, C. C., Evans, H. P., and Snidle, R. W., "Conditions for Scuffing Failure of Ground and Superfinished Steel Disks at High Sliding Speeds Using a Gas Turbine Engine Oil," *Journal of Tribology*, **117**(3), p. 482–489, 1995.

[10] Snidle, R. W., Dhulipalla, A. K., Evans, H. P., and Cooper, C. V., "Scuffing Performance of a Hard Coating Under EHL Conditions at Sliding Speeds up to 16 m/s and Contact Pressures up to 2.0 GPa," *Journal of Tribology*, **130**(2), p. 1–10, 2008.

[11] Clerico, M., "A Study of the Friction and Wear of Nylon Against Metal," *Wear*, **13**(3), p. 183–197, 1969.

[12] Gordon, D. H., and Kukureka, S. N., "The Wear and Friction of Polyamide 46 and Polyamide 46/Aramid-Fibre Composites in Sliding-Rolling Contact," *Wear*, **267**(1–4), p. 669–678, 2009.

[13] Xu, H., Kahraman, A., Anderson, N. E., and Maddock, D. G., "Prediction of Mechanical Efficiency of Parallel-Axis Gear Pairs," *Journal of Mechanical Design, Transactions of the ASME*, **129**(1), p. 58–68, 2007.

[14] Talbot, D. C., "An Experimental and Theoretical Investigation of the Efficiency of Planetary Gear Sets," Ph. D. Dissertation, The Ohio State University, Columbus,

Ohio, 2012.

[15] Petry-Johnson, T. T., Kahraman, A., Anderson, N. E., and Chase, D. R., "An Experimental Investigation of Spur Gear Efficiency," *Journal of Mechanical Design, Transactions of the ASME,* **130**(6), p. 0626011–06260110, 2008.

[16] Diab, Y., Ville, F., and Velex, P., "Prediction of Power Losses Due to Tooth Friction in Gears," *Tribology Transactions*, **49**(2), p. 260–270, 2006.

[17] Shon, S., "An Experimental Study on the Impact of Various Surface Treatments on Friction, Scuffing and Wear Characteristics of Lubricated Rolling-Sliding Contacts," M.S Thesis, The Ohio State University, Columbus, Ohio, 2012.

[18] Benedict, G. H., and Kelley, B. W., "Instantaneous Coefficients of Gear Tooth Friction," *ASLE Transactions*, **4**(1), p. 59–70, 1961.

[19] Drozdov, Y. N., and Gavrikov, Y. A., "Friction and Scoring Under the Conditions of Simultaneous Rolling and Sliding of Bodies," *Wear,* **11**(4), p. 291–302, 1968.

[20] O'Donoghue, J. P., and Cameron, A., "Friction and Temperature in Rolling Sliding Contacts," *ASLE Transactions,* **9**(2), p. 186–194, 1966.

[21] Xu, H., "Development of a Generalized Mechanical Efficiency Prediction Methodology for Gear Pairs," Ph.D. Dissertation, The Ohio State University, Columbus, Ohio, 2005.

[22] International Organization for Standardization, "Gears - FZG Test Procedures - Part 1: FZG Test Method A/8,3/90 for Relative Scuffing Load-Carrying Capacity Oils,"

ISO 14635-1:2000, 2010.